Structures, Magnetic Properties, and Reactivity Studies of Salts Containing the Dinuclear Anion $[M_2Cl_6]^{2-}$ (M = Mn, Fe, Co)

Jui-Sui Sun,[†] Hanhua Zhao,[†] Xiang Ouyang,[†] Rodolphe Clérac,[†] Jennifer A. Smith,[†] Juan M. Clemente-Juan,[‡] Carlos Gómez-Garcia,[‡] Eugenio Coronado,[‡] and Kim R. Dunbar*[,†]

Center for Fundamental Materials Research, Department of Chemistry, Michigan State University, East Lansing, Michigan 48824, and Departamento Química Inorgánica, Universitat de Valencia, E-46100 Burjassot, Valencia, Spain

Received May 13, 1999

Salts of the edge-sharing bitetrahedral anion $[M_2Cl_6]^{2-}$ with M = Mn, Fe, and Co were prepared in high yields by reaction of MCl_2 with 1 equiv of chloride ion. The anion $[Fe_2Cl_6]^{2-}$ was isolated with five different cations, namely, $[PPh_4]^+$ (**1**), $[Et_4N]^+$ (**2**), $[ppn]^+$ (**3**), $[AsPh_4]^+$ (**4**), and [H-TMPP]$^+$ (**5**) ([H-TMPP]$^+$ = tris(2,4,6-trimethoxyphenyl)phosphonium; $[ppn]^+$ = bis(triphenylphosphonium)iminium chloride). The Mn and Co compounds were isolated as $[ppn]^+$ salts, $[ppn]_2[Co_2Cl_6]$ (**6**) and $[ppn]_2[Mn_2Cl_6]$ (**7**). The compounds were characterized by single-crystal X-ray analysis and subjected to variable-temperature and field-dependent magnetic measurements. These magnetic data were analyzed from a spin Hamiltonian that contains an isotropic exchange term supplemented by a zero-field-splitting term to account for the single-ion anisotropy of the interacting spins. By using this approach, the $[Fe_2Cl_6]^{2-}$ salts (**1**−**5**) were shown to exhibit magnetic behavior dominated by single-ion anisotropy of the spin $S = 2$ of the tetrahedral Fe(II) ions ($D \sim 5$ cm^{-1}). The Co(II) compound (**6**) was found to exhibit considerable single-ion anisotropy of the spin $S = {}^3/_2$ tetrahedral Co(II) centers ($D = 29$ cm^{-1}) and stronger antiferromagnetic coupling than the Fe compounds. In the absence of complicating factors such as ZFS effects, as is the case for the Mn(II) derivative (**7**) it was possible to discern weak intermolecular as well as intramolecular antiferromagnetic interactions. Reactions between 2,2′-bipyrimidine (2,2′-bpym) and salts of $[Fe_2Cl_6]^{2-}$ yielded two neutral compounds, namely, $Fe_2Cl_4(2,2'\text{-bpym})_3$ (**8**) and $[Et_4N]Cl\cdot[Fe_2Cl_4(MeOH)_4(\mu\text{-}2,2'\text{-bpym})]$ (**9**). In contrast to the previously described Fe(II) compounds, the Fe(II) center is octahedral in **8** and **9**. The electronic ground state of this ion is orbitally degenerate and therefore highly anisotropic. An analysis of the magnetic data confirmed these predictions and revealed that the bridging ligand mediates antiferromagnetic exchange of ∼1 cm^{-1} and that the D parameter is large and negative ($D \sim -17$ cm^{-1}).

I. Introduction

High-spin polynuclear transition metal compounds are of interest for their magnetic properties in biological[1] as well as materials chemistry.[2] With respect to iron compounds, the magnetic behavior of dinuclear and polynuclear ferrous systems has not been well-investigated compared to ferric systems. This is due, in part, to the large zero-field splittings and substantial anisotropies of the magnetic hyperfine interactions, which lend interesting properties to the compounds but which also render it difficult to fit the magnetic data due to the large number of parameters involved.

A number of years ago in our laboratories, we reported a reaction between anhydrous ferric chloride and a basic phosphine ligand that led to the reduction of Fe^{III} to Fe^{II} and formation of $[Fe_2Cl_6]^{2-}$, a hitherto unknown binary ferrous chloride.[3a] This discovery led us to investigate whether the $[Fe_2Cl_6]^{2-}$ unit or related dinuclear compounds would be accessible directly from the polymeric halides MCl_2 (M = Mn, Fe, Co, Ni). The primary impetus for this investigation is to

[†] Michigan State University. Current address: Texas A&M University.
[‡] Universitat de València.

(1) (a) Holm, R. H. *Acc. Chem. Res.* **1977**, *10*, 427. (b) Holm, R. H. *Chem. Soc. Rev.* **1981**, *10*, 455. (c) Papaefthymiou, V.; Girerd, J. J.; Moura, I.; Moura, J. J. G.; Münck, E. *J. Am. Chem. Soc.* **1987**, *109*, 4703. (d) Taft, K. L.; Lippard, S. J. *J. Am. Chem. Soc.* **1990**, *112*, 9629. (e) Ménage, S.; Vincent, J. M.; Lambeaux, C.; Chottard, G.; Grand, A.; Fontecave, M. *Inorg. Chem.* **1993**, *32*, 4766. (f) Taft, K. L.; Papaefthymiou, G. C.; Lippard, S. J. *Science* **1993**, *259*, 1302. (g) Zang, Y.; Jang, H. G.; Chiou, Y. M.; Hendrich, M. P.; Que, L., Jr. *Inorg. Chim. Acta* **1993**, *213*, 41. (h) Hendrich, M. P.; Day, E. P.; Wang, C.-P.; Synder, B. S.; Holm, R. H.; Münck, E. *Inorg. Chem.* **1994**, *33*, 2848 and references therein. (i) Powell, A. K.; Heath, S. L. *Comments Inorg. Chem.* **1994**, *15*, 255 and references therein. (j) Goldberg, D. P.; Tesler, J.; Bastos, C. M.; Lippard, S. J. *Inorg. Chem.* **1995**, *34*, 3011.

(2) (a) Willett, R. D.; Landee, C. P.; Gaura, R. M.; Swank, D. D.; Groenedijk, H. A.; van Duynevelt, A. J. *J. Magn. Magn. Mater.* **1980**, *15*−*18*, 1055. (b) Groenedijk, H. A.; van Duynevelt, A. J.; Blöte, H. W. J.; Gaura, R. M.; Willett, R. D. *Physica* **1981**, *106B*, 47. (c) Kitajima, N.; Amagai, H.; Tamura, N.; Ito, M.; Moro-oka, Y.; Heerwegh, K.; Pénicaud, A.; Mathur, R.; Reed, C. A.; Boyd, P. D. W. *Inorg. Chem.* **1993**, *32*, 3583. (d) Taft, K. L.; Delfs, C. D.; Papaefthymiou, G. C.; Foner, S.; Gatteschi, D.; Lippard, S. J. *J. Am. Chem. Soc.* **1994**, *116*, 823 and references therein. (e) Elmali, A.; Elerman, Y.; Svoboda, I.; Fuess, H.; Griesar, K.; Haase, W. *Z. Naturforsch.* **1994**, *49B*, 365. (f) Mathonière, C.; Carling, S. G.; Yusheng, D.; Day, P. *J. Chem. Soc., Chem. Commun.* **1994**, 1551. (g) Klose, A.; Solari, E.; Floriani, C.; Chiese-Villa, A.; Rizzoli, C.; Re, N. *J. Am. Chem. Soc.* **1994**, *116*, 9123. (h) Aromi, G.; Claude, J. P.; Knapp, M. J.; Huffman, J. C.; Hendrickson, D. N.; Christou, G. *J. Am. Chem. Soc.* **1998**, *120*, 2977.

(3) (a) Dunbar, K. R.; Quillevéré, A. *Angew. Chem., Int. Ed. Engl.* **1992**, *31*, 1360. (b) Ruhlandt-Senge, K.; Müller, U. *Z. Naturforsch* **1992**, *47B*, 1075. (c) Dunbar, K. R.; Quillevéré, A. *Polyhedron* **1993**, *12*, 807. (d) Dunbar, K. R.; Sun, J.-S. *Mol. Cryst. Liq. Cryst.* **1995**, *274*, 51.

10.1021/ic990525w CCC: $18.00
Published on Web 11/20/1999

access discrete, soluble forms of high-spin complexes for use as building blocks in larger clusters or arrays. In this vein, we have performed reactions of the $[Fe_2Cl_6]^{2-}$ salts with 2,2′-bipyrimidine (2,2′-bpym), a bis-chelating ligand that is capable of transmitting electronic and magnetic information between metal centers.[4] Herein we report the syntheses, structural characterization, and magnetic studies of various salts of the dinuclear anions $[M_2Cl_6]^{2-}$ (M = Mn, Fe, and Co) and the products of reactions between bipyrimidine and $[Fe_2Cl_6]^{2-}$ to give $Fe_2Cl_4(2,2'\text{-bpym})_3$ and $[Et_4N]Cl\cdot[Fe_2Cl_4(MeOH)_4(\mu\text{-}2,2'\text{-bpym})]$. A portion of this work has been published in a preliminary format.[3d]

II. Experimental Section

Physical Measurements. Infrared spectra were recorded on a Nicolet 740 FT-IR spectrophotometer. Elemental analyses were performed at Desert Analysis, Tucson, AZ. Variable-temperature susceptibility measurements were carried out in the temperature range 2−300 K at a magnetic field of 0.1 T using a magnetometer (Quantum Design MPMS-5) equipped with a SQUID sensor. Isothermal magnetization measurements were performed as a function of the external magnetic field up to 5 T at 2 and 5 K. Magnetization was also measured as a function of temperature at different fields (2, 4, and 5 T). After correcting for the diamagnetism of the Fe(II) samples, calculated from Pascal's constants, an additional temperature-independent paramagnetic (TIP) correction was subtracted in order to obtain an approximately constant value of the χT product at high temperatures (above 100 K). This TIP was in the range 0.0005−0.0009 emu/mol.

Procedures and Starting Materials. The starting materials $MnCl_2$, $FeCl_2$, and $CoCl_2$ were purchased from Strem Chemicals, Inc., and used without further purification. Tris(2,4,6-trimethoxyphenyl)phosphine (TMPP) was prepared according to published methods or purchased from Aldrich and used without further purification.[5] [H-TMPP]Cl was prepared by the reaction of TMPP with HCl.[6] $[PPh_4]Cl$ (tetraphenylphosphonium chloride) and $[AsPh_4]Cl$ (tetraphenylarsonium chloride) were purchased from Lancaster Synthesis, $[Et_4N]Cl$ (tetraethylammonium chloride) was purchased from Sigma Chemical Co., and [ppn]Cl (ppn = bis(triphenylphosphonium)iminium chloride) was purchased from Aldrich; all were used as received. Acetone was distilled over 3 Å molecular sieves. Diethyl ether, hexanes, and THF were distilled over sodium−potassium/benzophenone, whereas methanol was distilled over $Mg(OMe)_2$ under a nitrogen atmosphere. Unless otherwise specified, all reactions were carried out under an argon atmosphere by using standard Schlenk-line techniques. Due to the extreme moisture sensitivity of these compounds, all glassware was pretreated with the commercially available reagent Glassclad.

Syntheses of $[Fe_2Cl_6]^{2-}$ Salts. (i) Preparation of $[PPh_4]_2[Fe_2Cl_6]$ (1). An acetone solution (15 mL) of $[PPh_4]Cl$ (0.887 g, 2.367 mmol) was added to 15 mL of an acetone solution of $FeCl_2$ (0.300 g, 2.367 mmol), and the resulting solution was stirred for 12 h to give a pale yellow precipitate and a yellow solution. The solution was filtered through Celite along with acetone washings (20 mL) of the precipitate. After concentration of the filtrate, diethyl ether (15 mL) was added to produce an off-white compound: yield, 0.854 g (72% based on $FeCl_2$). IR (Nujol, cm^{-1}): 1585 (w), 1483 (w), 1436 (ms), 1338 (w), 1313 (w), 1161 (w), 1109 (s, br), 1071 (m), 1028 (m), 995 (m), 758 (ms), 749 (m, sh), 720 (s), 687 (s), 616 (w), 525 (s, br), 447 (w); ν(FeCl) 340 (ms), 290 (m), 238 (m). Anal. Calcd for $Fe_2Cl_6P_2C_{48}H_{40}$: C, 57.47; H, 4.02; Cl, 21.20. Found: C, 57.08; H, 3.88; Cl, 21.03.

(ii) Preparation of $[Et_4N]_2[Fe_2Cl_6]$ (2). The compound $[Et_4N]_2[Fe_2Cl_6]$ was prepared in a manner identical to that described in (i) from the reaction of $[Et_4N]Cl$ (0.327 g, 1.972 mmol) and $FeCl_2$ (0.250 g, 1.972 mmol) in acetone; yield, 0.426 g (74% based on $FeCl_2$). IR (Nujol, cm^{-1}): 1404 (m), 1305 (m), 1184 (s), 1081 (m), 1033 (s, br), 1006 (ms, br), 801 (s, br), 467 (w); ν(FeCl) 379 (m), 344 (s), 298 (s), 240 (s). Repeated attempts to obtain analytical data were unsuccessful due to the extreme air and moisture sensitivity of the compound.

(iii) Preparation of $[ppn]_2[Fe_2Cl_6]$ (3). The salt $[ppn]_2[Fe_2Cl_6]$ was prepared in a manner identical to that described in (i) from the reaction of [ppn]Cl (0.453 g, 0.789 mmol) and $FeCl_2$ (0.100 g, 0.789 mmol) in acetone; yield, 0.415 g (75% based on $FeCl_2$). IR (Nujol, cm^{-1}): 1586 (w), 1480 (m), 1438 (m), 1265 (s, br), 1178 (w), 1166 (w), 1114 (s, br), 1026 (w), 997 (m), 801 (w), 796 (w, sh), 757 (w, sh), 747 (m), 720 (s), 691 (s), 549 (s), 530 (s), 499 (s); ν(FeCl) 395 (m), 346 (s), 294 (s), 237 (s). Anal. Calcd for $Fe_2Cl_6N_2P_4C_{72}H_{60}$: C, 61.70; H, 4.31; Cl, 15.18. Found: C, 61.85; H, 4.32; Cl, 15.02.

(iv) Preparation of $[AsPh_4]_2[Fe_2Cl_6]$ (4). The compound $[AsPh_4]_2[Fe_2Cl_6]$ was prepared in a manner identical to that described in (i) from the reaction of $[AsPh_4]Cl$ (0.185 g, 0.442 mmol) and $FeCl_2$ (0.056 g, 0.442 mmol) in acetone; yield, 0.185 g (77% based on $FeCl_2$). IR (Nujol, cm^{-1}): 1570 (w), 1483 (w), 1438 (m), 1336 (w), 1310 (w), 1185 (w), 1162 (w), 1082 (s), 1022 (w), 996 (m), 750 (s), 738 (s), 686 (s), 614 (w), 476 (s), 459 (s); ν(Fe−Cl) 340 (s, br), 289 (m), 239 (m). Anal. Calcd for $Fe_2Cl_6As_2C_{48}H_{40}$: C, 52.84; H, 3.70; Cl, 19.50. Found: C, 53.86; H, 3.68; Cl, 20.21.

(v) Preparation of $[H\text{-}TMPP]_2[Fe_2Cl_6]$ (5). The compound $[H\text{-}TMPP]_2[Fe_2Cl_6]$ was prepared in a manner identical to that described in (i) from the reaction of [H-TMPP]Cl (0.370 g, 0.650 mmol) and $FeCl_2$ (0.082 g, 0.650 mmol) in acetone; yield, 0.365 (81% based on $FeCl_2$). IR (Nujol, cm^{-1}): 1594 (s), 1577 (s), 1410 (m), 1338 (m), 1305 (w), 1230 (m), 1206 (s), 1180 (w), 1157 (m), 1133 (m), 1100 (m), 1023 (m), 948 (w), 927 (w), 913 (w), 884 (w), 819 (w), 643 (w); ν-(FeCl) 340 (ms), 290 (m), 238 (m). Anal. Calcd for $Fe_2Cl_6P_2O_{18}C_{54}H_{68}$: C, 46.61; H, 4.92; Cl, 15.28. Found: C, 45.98; H, 4.90; Cl, 15.27.

Syntheses of $[ppn]_2[M_2Cl_6]$ (M = Mn, Co). (i) Preparation of $[ppn]_2[Co_2Cl_6]$ (6). Anhydrous $CoCl_2$ (0.260 g, 2 mmol) and [ppn]Cl (1.144 g, 2 mmol) were dissolved in 60 mL of acetone and stirred at room temperature for 16 h. A blue solution and a large quantity of blue solid were present at the end of this time. The blue product was collected by filtration, and the filtrate was treated with 40 mL of diethyl ether to yield additional microcrystalline product; combined yield, 1.0175 g (67%). IR (Nujol, cm^{-1}): 1705 (ms), 1587 (m), 1261 (br), 1111 (m), 1026 (m), 997 (m), 798 (m), 762 (m), 742 (m), 690 (s), 550 (s), 532 (s), 495 (s), 395 (ms), 333 (ms), 306 (ms), 268 (br). Anal. Calcd for $Co_2Cl_6P_4N_2C_{72}H_{60}$: C, 61.43; H, 4.30; N, 1.99. Found: C, 61.46; H, 4.37; N, 1.79.

(ii) Preparation of $[ppn]_2[Mn_2Cl_6]$ (7). Anhydrous $MnCl_2$ (0.252 g, 2 mmol) and [ppn]Cl (1.145 g, 2 mmol) were dissolved in 35 mL of acetone and stirred for 16 h. The resulting colorless solution was filtered to remove any insoluble particulates, and the filtrate was treated with 40 mL of diethyl ether to give a pale yellow-green microcrystalline product, which was collected, washed with 5 mL of diethyl ether, and dried in vacuo; yield, 1.14 g (97%). IR (Nujol, cm^{-1}): 1707 (m), 1587 (m), 1265 (br), 1180 (m), 1113 (ms), 1026 (m), 997 (s), 800 (ms), 748 (s), 694 (s), 551 (s), 532 (s), 499 (s), 396 (ms), 330 (s), 287 (ms), 248

(4) (a) Bly, D. D.; Mellon, M. G. *Anal. Chem.* **1963**, *35*, 1386. (b) Dose, E. V.; Wilson, L. J. *Inorg. Chem.* **1978**, *17*, 2660. (c) Petty, R. H.; Welch, B. R.; Wilson, L. J.; Bottomly, L. A.; Kadish, K. M. *J. Am. Chem. Soc*. **1980**, *102*, 611. (d) Ruminski, R. R.; Petersen, J. D. *Inorg. Chem.* **1982**, *21*, 3706. (e) Ruminski, R. R.; Van Tassel, K. D.; Petersen, J. D. *Inorg. Chem.* **1984**, *23*, 4380. (f) Brewer, G.; Sinn, E. *Inorg. Chem.* **1985**, *24*, 4580. (g) Morgan, L. W.; Goodwin, K. V.; Pennington, W. T.; Petersen, J. D. *Inorg. Chem.* **1992**, *31*, 1103. (h) De Munno, G.; Julve, M.; Lloret, F.; Faus, J.; Verdaguer, M.; Caneschi, A. *Angew. Chem., Int. Ed. Engl.* **1993**, *32*, 1046. (i) De Munno, G.; Viterbo, D.; Caneschi, A.; Lloret, F.; Julve, M. *Inorg. Chem.* **1994**, *33*, 1585. (j) De Munno, G.; Poerio, T.; Viau, G.; Julve, M.; Lloret, F.; Journaux, Y.; Riviere, E. *Chem. Commun.* **1996**, 2587. (k) De Munno, G.; Poerio, T.; Julve, M.; Lloret, F.; Viau, G.; Caneschi, A. *J. Chem. Soc., Dalton Trans.* **1997**, 601. (l) Cortes, R.; Urtiaga, M. K.; Lezama, L.; Pizarro, J. L.; Arriortua, M. I.; Rojo, T. *Inorg. Chem.* **1997**, *36*, 5016. (m) De Munno, G.; Ventura, W.; Viau, G.; Lloret, F.; Faus, J.; Julve, M. *Inorg. Chem.* **1998**, *37*, 1458.

(5) (a) Protopopov, I. S.; Kraft, M. Ya. *Zh. Obshch. Khim.* **1963**, *33*, 3050. (b) Protopopov, I. S.; Kraft, M. Ya. *Med. Promst. SSSR* **1959**, *13*, 5. (c) Dunbar, K. R.; Haefney S. C. *Polyhedron* **1994**, *13*, 727.

(6) Preparation of [H-TMPP]Cl: Addition of dilute HCl into a benzene solution of TMPP resulted in an immediate precipitation of a white solid. The reaction mixture was stirred for 30 min at room temperature. A white solid ([H-TMPP]Cl) was collected after filtration and was washed with diethyl ether and dried in vacuo in nearly quantitative yield.

Table 1. Crystallographic Information for **1**−**4** and **8**[a]

	1	**2**	**3**	**4**	**8**
formula	$Fe_2Cl_6P_2C_{48}H_{40}$	$Fe_2Cl_6N_2C_{16}H_{40}$	$Fe_2Cl_6P_4N_2C_{72}H_{60}$	$Fe_2C1_6C_{48}As_2H_{40}$	$Fe_2Cl_4C_{24}N_{12}H_{18}$
fw	1003.20	584.92	1401.59	1091.10	727.99
T (K)	173(1)	173(1)	188(1)	173(1)	189(1)
space group	$P\bar{1}$	$P2_1/n$	$P2_1/n$	$P\bar{1}$	$P\bar{1}$
a, Å	9.801(2)	8.738(3)	21.618(6)	9.802(2)	7.047(1)
b, Å	12.961(2)	10.210(3)	13.189(4)	13.070(3)	7.352(2)
c, Å	9.658(2)	15.554(4)	23.89(1)	9.736(2)	14.905(4)
α, deg	94.34(2)	90	90	94.23(2)	100.61(2)
β, deg	100.16(2)	104.09(2)	102.63(3)	99.58(2)	90.27(2)
γ, deg	108.65(1)	90	90	108.71(2)	111.99(2)
V, Å^3	1132.7(9)	1345.9(7)	6646(8)	1154.0(4)	701.5(6)
Z	1	2	4	1	1
μ (mm^{-1})	1.100	1.685	0.817	2.432	1.458
d_{calc}, g/cm^3	1.470	1.443	1.401	1.570	1.723
radiation	Mo Kα graphite monochromated ($\lambda_\alpha = 0.71073$)				
total data	4246	2686	10685	3632	2272
unique data	3988	2513	10353	3402	2078
R	0.027	0.027	0.080	0.027	0.032
R_w	0.043	0.038	0.080	0.035	0.039
GOF	2.06	1.68	2.94	1.50	1.39

[a] $R = \sum[||F_o| - |F_c||]/\sum|F_o|$. $R_w = [\sum w(|F_o| - |F_c|)^2/\sum wF_o^2]^{1/2}$. GOF $= [\sum w(|F_o| - |F_c|)^2/(N_{obs} - N_{parameters})]^{1/2}$.

(ms), 228 (ms). Anal. Calcd for $Mn_2Cl_6P_4N_2C_{72}H_{60}$: C, 61.78; H, 4.32; N, 2.00. Found: C, 61.65; H, 4.56; N, 1.74.

Syntheses of 2,2′-Bipyrimidine Compounds. (i) $Fe_2Cl_4(2,2'\text{-bpym})_3$ (8). A bulk sample of $Fe_2Cl_4(2,2'\text{-bpym})_3$ was obtained by the addition of an acetone solution (15 mL) of 2,2′-bpym (0.075 g, 0.473 mmol) to an acetone solution (15 mL) of $FeCl_2$ (0.040 g, 0.316 mmol). The solution was stirred for 12 h at room temperature to yield a red-orange solution and a dark gray precipitate. The solution was decanted by cannula techniques and discarded, and the solid was washed with MeOH, acetone, and diethyl ether and dried in vacuo to give a dark gray compound (yield: 0.053 g, 46% based on $FeCl_2$). IR (Nujol, cm^{-1}): 1588 (w), 1572 (m), 1555 (mw, br), 1404 (s), 1140 (vw), 1018 (vw), 1006 (vw), 834 (w), 827 (w), 761 (mw), 753 (w), 686 (mw), 658 (mw); ν(FeCl) 302 (vw), 265 (w, sh), 253 (m), 227 (w, br). The same compound was prepared as black-purple, single crystals by slow diffusion of a MeOH solution of $[PPh_4]_2[Fe_2Cl_6]$ into a THF solution of 2,2′-bpym. Anal. Calcd for $Fe_2Cl_4N_{12}C_{24}H_{18}$: C, 39.60; H, 2.49. Found: C, 38.72; H, 3.13.

(ii) $[Et_4N]Cl\cdot[Fe_2Cl_4(MeOH)_4(\mu\text{-}2,2'\text{-bpym})]$ (9). A bulk sample of $[Et_4N]Cl\cdot[Fe_2Cl_4(MeOH)_4(\mu\text{-}2,2'\text{-bpym})]$ was obtained by the addition of a methanol solution (15 mL) of 2,2′-bpym (0.0220 g) to $[Et_4N]_2[Fe_2Cl_6]$ (0.1629 g) in methanol. The resulting solution was stirred for 12 h at room temperature to give a pale red solution. The solution was concentrated down to yield a black solution. The addition of diethyl ether (40 mL) resulted in a black compound (yield: 0.0352 g, 36% based on 2,2′-bpym). IR (Nujol, cm^{-1}): 3306 (m), 1574 (ms), 1404 (m), 1309 (m), 1261 (m), 1184 (m), 1080 (w), 1030 (m), 1006 (m), 891 (w), 852 (w), 794 (m), 756 (w), 686 (w), 667 (w). Due to the lability of the axial methanol molecules and air sensitivity, a satisfactory elemental analysis could not be obtained.

III. X-ray Crystallographic Studies

Crystallographic data for compounds **1**, **2**, **4**, and **8** were collected on a Rigaku AFC6S diffractometer, data for **3** were collected on a Nicolet P3/V diffractometer, and data for **6**, **7**, and **9** were collected on a SMART CCD diffractometer. All three instruments are equipped with monochromated Mo Kα radiation. Crystallographic computing was performed on a VAXSTATION 4000 by using the Texsan crystallographic software package of Molecular Structure Corporation for **1**−**4** and **8**[7a] and on a Silicon Graphics computer using the SHELXTL programs from Bruker AXS for **6**, **7**, and **9**.[7b] Crystal parameters and basic information pertaining to data collection and structure refinement are summarized in Tables 1 and 2. Selected bond distances and angles are listed in Tables 3−10.

Table 2. Crystallographic Information for **6**, **7**, and **9**[a]

	6	**7**	**9**
formula	$C_{72}H_{60}Cl_6Co_2N_2P_4$	$C_{72}H_{60}Cl_6Mn_2N_2P_4$	$C_{40}H_{84}Cl_{10}Fe_4N_{10}O_8$
fw	1407.66	1399.68	1411.07
T (K)	173(2)	133(2)	173(2)
space group	$P2_1/n$	$P2_1/n$	$P2_1/c$
a, Å	21.6564(2)	21.7045(4)	13.589(2)
b, Å	13.1996(2)	13.2667(2)	15.262(2)
c, Å	23.8566(1)	24.0041(3)	15.423(2)
α, deg	90	90	90
β, deg	102.73(1)	102.549(1)	94.318(3)
γ, deg	90	90	90
V, Å^3	6651.89(12)	6746.79(18)	3189.7(8)
Z	4	4	2
μ (mm^{-1})	0.880	0.750	1.361
d_{calc}, g/cm^3	1.406	1.378	1.469
radiation	Mo Kα graphite monochromated ($\lambda_\alpha = 0.71073$)		
total data	40634	41252	37705
unique data	15565	15889	7774
R1	0.0532	0.0411	0.0642
wR2	0.0802	0.0815	0.1396
GOF	0.948	1.175	0.910

[a] R1 $= \sum[||F_o| - |F_c||]/\sum|F_o|$. wR2 $= \{\sum[w(F_o^2 - F_c^2)^2]/\sum[w(F_o^2)^2]\}^{1/2}$. GOF $= \{\sum[w(F_o^2 - F_c^2)^2]/(n - p)\}^{1/2}$ where n = total number of reflections and p = total number of parameters.

$[PPh_4]_2[Fe_2Cl_6]$ (1). Single crystals of $[PPh_4]_2[Fe_2Cl_6]$ were grown by a slow diffusion of hexanes into an acetone solution of the title compound. A pale yellow crystal of dimensions 0.62 × 0.89 × 0.62 mm^3 was secured on the tip of a glass fiber with Dow Corning silicone grease and placed in a cold N_2(g) stream. Least-squares refinement using 23 well-centered reflections in the range $34.3° \le 2\theta \le 38.2°$ defined a triclinic crystal system. The data were collected at 173(1) K using the $\omega-2\theta$ scan technique to a maximum 2θ value of 50°. A total of 4246 reflections were collected, 3988 of which were unique. An empirical absorption correction based on azimuthal scans of three reflections was applied which resulted in transmission factors ranging from 0.89 to 1.00, and the data were corrected for Lorentz and polarization effects. The structure was solved

(7) (a) TEXSAN-TEXRAY Structure Analysis Package, Molecular Structure Corporation, 1985. (b) Calculations were done on a Silicon Graphics Indigo workstation, VAXSTATION 4000 computer or VAX 11/780 computer at the Department of Chemistry, Michigan State University with the SHELXTL 5.0 or the VAX-SDP software package.

Table 3. Selected Bond Distances and Bond Angles for $[PPh_4]_2[Fe_2Cl_6]$ (**1**)

Bond Distances

A	B	A−B (Å)	A	B	A−B (Å)
Fe1	Fe1*	3.4517(9)	P1	C1	1.793(2)
Fe1	Cl1	2.2653(9)	P1	C7	1.799(2)
Fe1	Cl2	2.4048(8)	P1	C13	1.796(2)
Fe1	Cl2*	2.4021(9)	P1	C19	1.791(2)
Fe1	Cl3	2.2540(8)			

Bond Angles

A	B	C	A−B−C (deg)	A	B	C	A−B−C (deg)
Cl1	Fe1	Cl2	110.01(3)	C1	P1	C7	111.0(1)
Cl1	Fe1	Cl2*	112.16(3)	C1	P1	C13	106.4(1)
Cl1	Fe1	Cl3	118.86(3)	C1	P1	C19	110.3(1)
Cl2	Fe1	Cl2*	88.21(3)	C7	P1	C13	110.7(1)
Cl2	Fe1	Cl3	110.95(3)	C7	P1	C19	106.4(1)
Fe1	Cl2	Fe1*	91.79(3)	C13	P1	C19	112.0(1)

Table 4. Selected Bond Distances and Bond Angles for $[Et_4N]_2[Fe_2Cl_6]$ (**2**)

Bond Distances

A	B	A−B (Å)	A	B	A−B (Å)
Fe1	Fe1*	3.4232(9)	N1	C1	1.517(3)
Fe1	Cl1	2.252(1)	N1	C3	1.525(3)
Fe1	Cl2	2.392(1)	N1	C5	1.518(3)
Fe1	Cl2*	2.4027(9)	N1	C7	1.522(3)
Fe1	Cl3	2.2440(9)			

Bond Angles

A	B	C	A−B−C (deg)	A	B	C	A−B−C (deg)
Cl1	Fe1	Cl3	116.74(4)	C1	N1	C3	108.3(2)
Cl1	Fe1	Cl2	110.53(4)	C1	N1	C5	111.3(2)
Cl1	Fe1	Cl2*	112.33(3)	C1	N1	C7	108.4(2)
Cl3	Fe1	Cl2	113.27(3)	C3	N1	C5	108.9(2)
Cl3	Fe1	Cl2*	111.83(3)	C3	N1	C7	111.2(2)
Cl2	Fe1	Cl2*	88.88(3)	C5	N1	C7	108.8(2)
Fe1	Cl2	Fe1*	91.12(3)				

Table 5. Selected Bond Distances and Bond Angles for $[ppn]_2[Fe_2Cl_6]$ (**3**)

Bond Distances

A	B	A−B (Å)	A	B	A−B (Å)	A	B	A−B (Å)
Fe1	Fe1*	3.452(6)	Fe2	Fe2*	3.353(6)	N1	P1	1.61(1)
Fe1	Cl1	2.239(6)	Fe2	Cl4	2.235(6)	N1	P2	1.59(1)
Fe1	Cl2	2.418(5)	Fe2	Cl5	2.399(6)	N2	P3	1.60(1)
Fe1	Cl2*	2.387(6)	Fe2	Cl5*	2.388(6)	N2	P4	1.59(1)
Fe1	Cl3	2.252(6)	Fe2	Cl6	2.256(6)			

Bond Angles

A	B	C	A−B−C (deg)	A	B	C	A−B−C (deg)
Cl1	Fe1	Cl3	120.0(2)	Cl4	Fe2	Cl6	119.82(2)
Cl1	Fe1	Cl2	109.5(2)	Cl4	Fe2	Cl5	105.3(2)
Cl1	Fe1	Cl2*	110.4(2)	Cl4	Fe2	Cl5*	114.5(2)
Cl3	Fe1	Cl2	110.7(2)	Cl6	Fe2	Cl5	115.5(2)
Cl3	Fe1	Cl2*	113.5(2)	Cl6	Fe2	Cl5*	107.2(2)
Cl2	Fe1	Cl2*	88.2(2)	Cl5	Fe2	Cl5*	91.1(2)
Fe1	Cl2	Fe1*	91.8(2)	Fe2	Cl5	Fe2*	88.9(2)
P1	N1	P2	134(1)	P3	N2	P4	139(1)

by PHASE,[8] followed by DIRDIF84,[9] and refined by full-matrix least-squares refinement. All non-hydrogen atoms were refined anisotropically. The final full-matrix refinement was based on 3491 observed reflections with $F_o^2 > 3\sigma(F_o^2)$ that were used to fit 342 parameters to give $R = 0.027$ and $R_w = 0.043$. The goodness-of-fit index was 2.06, and the highest peak in the final difference map was 0.40 $e^-/Å^3$.

(8) PHASE: Calabrese, J. C. Patterson Heavy Atom Solution Extractor. Ph.D. Thesis, University of Wisconsin−Madison, 1972.

(9) DIRDIF84: Beurskens, P. T. Direct Methods for Difference Structures; Technical Report 1984/1; Crystallography Laboratory: Toernooiveld, 6525 Ed Nijmegen, The Netherlands, 1984.

Table 6. Selected Bond Distances and Bond Angles for $[AsPh_4]_2[Fe_2Cl_6]$ (**4**)

Bond Distances

A	B	A−B (Å)	A	B	A−B (Å)
Fe1	Fe1*	3.431(1)	As1	C1	1.914(4)
Fe1	Cl1	2.263(1)	As1	C7	1.916(4)
Fe1	Cl2	2.404(1)	As1	C13	1.915(4)
Fe1	Cl2*	2.402(1)	As1	C19	1.905(4)
Fe1	Cl3	2.256(1)			

Bond Angles

A	B	C	A−B−C (deg)	A	B	C	A−B−C (deg)
Cl1	Fe1	Cl2	109.28(5)	C1	As1	C7	110.8(2)
Cl1	Fe1	Cl2*	112.25(5)	C1	As1	C13	106.6(2)
Cl1	Fe1	Cl3	119.52(5)	C1	As1	C19	109.9(2)
Cl2	Fe1	Cl2*	88.88(4)	C7	As1	C13	111.1(2)
Cl2	Fe1	Cl3	110.48(5)	C7	As1	C19	106.4(2)
Fe1	Cl2	Fe1*	91.12(4)	C13	As1	C19	112.1(2)

Table 7. Selected Bond Distances and Bond Angles for $[ppn]_2[Co_2Cl_6]$ (**6**)

Bond Distances

A	B	A−B (Å)	A	B	A−B (Å)	A	B	A−B (Å)
Co1	Co1*	3.191(1)	Co2	Co2*	3.251(1)	N1	P1	1.585(3)
Co1	Cl2	2.224(1)	Co2	Cl5	2.232(1)	N1	P2	1.580(3)
Co1	Cl1	2.347(1)	Co2	Cl4	2.362(1)	N2	P3	1.585(3)
Co1	Cl1*	2.342(1)	Co2	Cl4*	2.334(1)	N2	P4	1.578(3)
Co1	Cl3	2.224(1)	Co2	Cl6	2.216(1)			

Bond Angles

A	B	C	A−B−C (deg)	A	B	C	A−B−C (deg)
Cl2	Co1	Cl3	115.94(4)	Cl5	Co2	Cl6	115.57(4)
Cl2	Co1	Cl1	106.86(4)	Cl5	Co2	Cl4	112.34(4)
Cl2	Co1	Cl1*	114.34(4)	Cl5	Co2	Cl4*	113.55(4)
Cl3	Co1	Cl1	114.81(2)	Cl6	Co2	Cl4	109.94(5)
Cl3	Co1	Cl1*	108.76(4)	Cl6	Co2	Cl4*	110.75(5)
Cl1	Co1	Cl1*	94.21(3)	Cl4	Co2	Cl4*	92.37(3)
Co1	Cl2	Co1*	85.79(3)	Co2	Cl5	Co2*	87.63(3)
P1	N1	P2	137.4(2)	P3	N2	P4	140.6(2)

Table 8. Selected Bond Distances and Bond Angles for $[ppn]_2[Mn_2Cl_6]$ (**7**)

Bond Distances

A	B	A−B (Å)	A	B	A−B (Å)	A	B	A−B (Å)
Mn1	Mn1*	3.344(1)	Mn2	Mn2*	3.408(1)	N1	P1	1.586(2)
Mn1	Cl1	2.305(1)	Mn2	Cl4	2.305(1)	N1	P2	1.583(2)
Mn1	Cl3	2.447(1)	Mn2	Cl6	2.466(1)	N2	P3	1.583(2)
Mn1	Cl3*	2.439(1)	Mn2	Cl6*	2.434(1)	N2	P4	1.582(2)
Mn1	Cl2	2.310(1)	Mn2	Cl5	2.316(1)			

Bond Angles

A	B	C	A−B−C (deg)	A	B	C	A−B−C (deg)
Cl1	Mn1	Cl2	118.00(3)	Cl4	Mn2	Cl5	118.21(3)
Cl1	Mn1	Cl3	105.58(3)	Cl4	Mn2	Cl6	108.63(3)
Cl1	Mn1	Cl3*	113.82(3)	Cl4	Mn2	Cl6*	110.04(3)
Cl2	Mn1	Cl3	114.49(3)	Cl5	Mn2	Cl6	111.52(3)
Cl2	Mn1	Cl3*	108.79(3)	Cl5	Mn2	Cl6*	113.40(3)
Cl3	Mn1	Cl3*	93.63(2)	Cl6	Mn2	Cl6*	91.87(2)
Mn1	Cl2	Mn1*	86.37(2)	Mn2	Cl5	Mn2*	88.13(2)
P1	N1	P2	137.3(2)	P3	N2	P4	141.2(1)

$[Et_4N]_2[Fe_2Cl_6]$ (2). Single crystals of $[Et_4N]_2[Fe_2Cl_6]$ were grown by slow diffusion of hexanes into an acetone solution of the compound. A pale yellow crystal of dimensions 0.67 × 0.45 × 0.37 mm^3 was secured on the tip of a glass fiber with Dow Corning silicone grease and placed in a cold N_2(g) stream. Least-squares refinement using 17 well-centered reflections in the range $39.5° \le 2\theta \le 39.9°$ indicated that the crystal belonged

Table 9. Selected Bond Distances and Bond Angles for $Fe_2Cl_4(2,2'\text{-bpym})_3$ (**8**)

Bond Distances

A	B	A−B (Å)	A	B	A−B (Å)
Fe1	Fe1*	5.918(2)	Fe1	N6	2.271(3)
Fe1	Cl1	2.402(1)	N1	C4	1.342(5)
Fe1	Cl2	2.391(1)	N2	C4	1.340(5)
Fe1	N1	2.208(3)	N3	C5	1.351(5)
Fe1	N3	2.218(3)	N4	C5	1.328(5)
Fe1	N5	2.224(3)	N5	C12	1.339(5)

Bond Angles

A	B	C	A−B−C (deg)	A	B	C	A−B−C (deg)
Cl1	Fe1	Cl2	102.77(5)	N1	Fe1	N3	74.7(1)
Cl1	Fe1	N1	95.27(9)	N1	Fe1	N5	171.2(1)
Cl1	Fe1	N3	90.3(1)	N1	Fe1	N6	99.4(1)
Cl1	Fe1	N5	91.51(9)	N3	Fe1	N5	99.7(1)
Cl1	Fe1	N6	164.03(8)	N3	Fe1	N6	87.5(1)
Cl2	Fe1	N3	162.35(9)	N5	Fe1	N6	73.3(1)

Table 10. Selected Bond Distances and Bond Angles for $[Et_4N]Cl\cdot[Fe_2Cl_4(MeOH)_4(\mu\text{-}2,2'\text{-bpym})]$ (**9**)

Bond Distances

A	B	A−B (Å)	A	B	A−B (Å)
Fe1	O2	2.139(4)	Fe2	O4	2.153(4)
Fe1	O1	2.164(4)	Fe2	O3	2.164(5)
Fe1	N1	2.236(5)	Fe2	N3	2.244(5)
Fe1	Cl1	2.3789(17)	Fe2	Cl3	2.3859(18)
Fe1	Cl2	2.3874(18)	Fe2	Cl4	2.3811(18)

Bond Angles

A	B	C	A−B−C (deg)	A	B	C	A−B−C (deg)
N2*	Fe1	N1	74.60(17)	N3	Fe2	N4*	73.64(17)
O2	Fe1	N1	86.85(16)	O4	Fe2	N3	85.71(17)
O1	Fe1	N1	84.61(16)	O3	Fe2	N3	85.68(18)
O1	Fe1	Cl1	92.89(13)	O3	Fe2	Cl3	94.43(14)
N1	Fe1	Cl1	90.63(13)	N3	Fe2	Cl3	92.94(13)
Cl1	Fe1	Cl2	102.19(6)	Cl4	Fe2	Cl5	102.46(6)

to the monoclinic crystal system. The data were collected at 173(1) K using the $\omega-2\theta$ scan technique to a maximum 2θ value of 50°. Of the 2686 reflections that were collected, 2513 were unique. An empirical absorption correction based on azimuthal scans of three reflections was applied which resulted in transmission factors ranging from 0.81 to 1.00. The data were corrected for Lorentz and polarization effects. The space group was determined to be $P2_1/n$ on the basis of the observed systematic absences. The structure was solved by PHASE,[8] followed by DIRDIF84[9] structure solution programs, and refined by full-matrix least-squares refinement. All non-hydrogen atoms were refined anisotropically. The final refinement was based on 1926 observed reflections with $F_o^2 > 3\sigma(F_o^2)$ that were used to fit 198 parameters to give $R = 0.027$ and $R_w = 0.038$. The goodness-of-fit index was 1.68, and the highest peak in the final difference map was 0.34 $e^-/Å^3$.

$[ppn]_2[Fe_2Cl_6]$ (3). Single crystals of $[ppn]_2[Fe_2Cl_6]$ were grown by slow diffusion of diethyl ether into a methanol solution of the compound. A pale yellow crystal of dimensions 0.26 × 0.34 × 0.29 mm^3 was secured on the tip of a glass fiber with Dow Corning silicone grease and placed in a cold N_2(g) stream. Least-squares refinement using 39 well-centered reflections in the range 5.5° ≤ 2θ ≤ 23.3° indicated a monoclinic crystal system. Data were collected at 188(1) K using the $\omega-2\theta$ scan technique to a maximum 2θ value of 47° and were corrected for Lorentz and polarization effects. Of the 10 685 reflections that were collected, 10 353 were unique. An empirical absorption correction based on azimuthal scans of three reflections was applied which resulted in transmission factors ranging from 0.89 to 1.09. The structure was solved by MITHRIL84[10] and DIRDIF84[9] structure solution programs and refined by full-matrix least-squares refinement. All non-hydrogen atoms were refined anisotropically except for atom N2 and some ring carbons of the $[ppn]^+$ ion due to the lack of data. The final refinement was based on 3890 observed reflections with $F_o^2 > 3\sigma(F_o^2)$ that were used to fit 630 parameters to give $R = 0.080$ and $R_w = 0.080$. The goodness-of-fit index was 2.94, and the highest peak in the final difference map was 0.80 $e^-/Å^3$.

$[AsPh_4]_2[Fe_2Cl_6]$ (4). Single crystals of $[AsPh_4]_2[Fe_2Cl_6]$ were grown by slow diffusion of hexanes into an acetone solution of the compound. A pale yellow crystal of dimensions 0.52 × 0.21 × 0.39 mm^3 was secured on the tip of a glass fiber with Dow Corning silicone grease and placed in a cold N_2(g) stream at 173(1) K. Least-squares refinement using 13 well-centered reflections in the range 39.4° ≤ 2θ ≤ 40.0° indicated that the crystal belonged to a triclinic crystal system. The $\omega-2\theta$ scan technique was used to collect data to a maximum 2θ value of 47°, which give 3402 unique reflections out of a total of 3632. An empirical absorption correction based on azimuthal scans of three reflections was applied which resulted in transmission factors ranging from 0.79 to 1.00. The data were corrected for Lorentz and polarization effects. The structure was solved by PHASE[8] and followed by DIRDIF84[9] structure solution programs in the $P\bar{1}$ space group. All non-hydrogen atoms were refined anisotropically. The final full-matrix refinement was based on 2682 observed reflections with $F_o^2 > 3\sigma(F_o^2)$ that were used to fit 342 parameters to give $R = 0.027$ and $R_w = 0.035$. The goodness-of-fit index was 1.50, and the highest peak in the final difference map was 0.28 $e^-/Å^3$.

$[ppn]_2[Co_2Cl_6]$ (6). Single crystals of $[ppn]_2[Co_2Cl_6]$ were grown by dissolving the compound in 20 mL of acetone and layering with 10 mL of hexanes in a Schlenk tube. Light blue crystals were harvested after 3 days. A light blue prism of approximate dimensions 0.05 × 0.04 × 0.02 mm was mounted on the tip of a glass fiber with Dow Corning silicone grease and placed in a cold N_2 stream at 173(2) K. Indexing and refinement of 53 reflections from a total of 60 frames with an exposure time of 10 s/frame indicated a monoclinic crystal system. A hemisphere of data with 1321 frames was collected with a scan width of 0.3° in ω and an exposure time of 30 s/frame. Indexing and refinement of 221 reflections from a total of 200 data frames generated a precise cell for data integration which led to 40 634 reflections in the range of $-28 \le h \le 18$, $-17 \le k \le 17$, $-31 \le l \le 31$ with a maximum 2θ angle of 56.60°. Final cell parameters were generated from the refinement of the centroid of 6220 strong reflections with $I > 10\sigma(I)$. The intensities were corrected for absorption and decay with the program SADABS,[11] which led to transmission factors between 0.89 and 1.00. Of the 15 565 unique reflections, a total of 8184 reflections with $I > 2\sigma(I)$ and $R_{int} = 0.0772$ remained after data reduction. Equivalent reflections were merged and truncated to a resolution of 0.85 Å to reduce the high R_{sigma} caused by the small size of the crystal. The structure was solved and refined with the use of the SHELXTL 5.04 package. The positions of all non-hydrogen atoms were located by direct methods and refined anisotropically by full-matrix least squares on F^2. Hydrogen atoms were placed in idealized positions. The final full-matrix refinement based on 11 293 unique reflections (merged and truncated) and 775 parameters led to R1 = 0.0532

(10) MITHRIL84: Gilmore, C. J. *J. Appl. Crystallogr.* **1984**, *17*, 42. University of Glasgow, Scotland.
(11) Sheldrick, G. M. *SADABS. Siemens Area Detector Absorption (and other) Correction*; University of Göttingen: Göttingen, Germany, 1998.

and wR2 = 0.0802 ($I > 2\sigma$). The goodness-of-fit is 0.948, and the highest peak in the final difference map is 0.491 $e^-/Å^3$.

[ppn]$_2$[Mn$_2$Cl$_6$] (7). Single crystals of **7** were obtained by layering a solution of the compound in 20 mL of acetone with 10 mL of hexanes in a Schlenk tube. Pale yellow crystals were harvested after 3 days. A crystal of approximate dimensions 0.49 × 0.31 × 0.26 mm^3 was mounted on the tip of a glass fiber with Dow Corning silicone grease and placed in a cold N_2 stream at 133(2) K. Indexing and refinement of 274 reflections from a total of 60 frames with an exposure time of 10 s/frame indicated a monoclinic crystal system. A hemisphere of data with 1321 frames was collected with a scan width of 0.3° in ω and an exposure time of 30 s/frame. Indexing and refinement of 297 reflections from a total of 100 data frames generated the precise cell for data integration which led to 41 252 reflections in the range of $-18 \le h \le 28$, $-17 \le k \le 14$, $-31 \le l \le 31$ with a maximum 2θ angle of 56.66°. Final cell parameters were generated from the refinement of the centroids of 8192 strong reflections with $I > 10\sigma$. The intensities were corrected for absorption and decay with the program SADABS, which led to transmission factors ranging from 0.83 to 1.00. Of the 15 889 unique reflections, a total of 11 647 reflections with $I > 2\sigma(I)$ and $R_{int} = 0.0321$ remained after data reduction. The data were solved and refined with the SHELXTL 5.04 package. The positions of all non-hydrogen atoms were located by direct methods and refined anisotropically by full-matrix least squares on F^2 whereas hydrogen atoms were placed in idealized positions. The final full-matrix refinement included 15 889 unique reflections used to fit 775 parameters, which led to R1 = 0.0407 and wR2 = 0.0768 ($I > 2\sigma$). The goodness-of-fit index is 1.036, and the highest peak in the final difference map is 0.493 $e^-/Å^3$.

Fe$_2$Cl$_4$(2,2′-bpym)$_3$ (8). Crystals of the product were grown by slow diffusion of a MeOH solution of [PPh$_4$]$_2$[Fe$_2$Cl$_6$] into a THF solution of 2,2′-bypyrimidine. A black-purple crystal of approximate dimensions 0.18 × 0.21 × 0.26 mm^3 was secured on the tip of a glass fiber with Dow Corning silicone grease and placed in a cold N_2(g) stream. Least-squares refinement using 25 well-centered reflections in the range $15.4° \le 2\theta \le 26.2°$ indicated the triclinic crystal system. Data were collected at 189(1) K using the $\omega-2\theta$ scan technique to a maximum 2θ value of 47°. The data, which were corrected for Lorentz and polarization effects, included 2272 reflections, 2078 of which were unique. An empirical absorption correction based on azimuthal scans of three reflections was applied which resulted in transmission factors ranging from 0.84 to 1.00. The space group was determined to be $P\bar{1}$. The structure was solved by MITHRIL84[10] and DIRDIF84[9] structure solution programs and refined by full-matrix least-squares refinement with all non-hydrogen atoms being refined anisotropically. The final refinement cycle was based on 1598 observed reflections with $F_o^2 > 3\sigma(F_o^2)$ that were used to fit 222 parameters to give $R = 0.032$ ($R_w = 0.039$) and a goodness-of-fit index of 1.39; the highest peak in the final difference map was 0.45 $e^-/Å^3$.

[Et$_4$N]Cl·[Fe$_2$Cl$_4$(MeOH)$_4$(μ-2,2′-bpym)] (9). Single crystals were grown by slow diffusion of a MeOH solution of [Et$_4$N]$_2$[Fe$_2$Cl$_6$] into a THF solution of 2,2′-bypyrimidine. A dark black-green crystal of dimensions 0.49 × 0.22 × 0.13 mm was secured on the tip of a glass fiber with Dow Corning silicone grease and placed in a cold N_2(g) stream on a CCD SMART system at 173(2) K. Indexing and refinement of 39 out of 79 reflections from a total of 60 frames with an exposure time of 10 s/frame indicated a monoclinic crystal system. A full sphere of data with 2474 frames was collected with a scan width of 0.3 in ω and an exposure time of 20 s/frame. A total of 37 705 reflections were collected in the range of $-18 < h < 18$, $-20 < k < 20$, $-20 < l < 20$ with a maximum 2θ angle of 56.68°. A reindexing of the reflection list with the TWINNING package written by R. Sparks indicated that the crystal is a rotational twin. It was found that there were 54 independent reflections in the reflection array that belong to component A and 9 independent reflections that belong to component B. Component B can be transformed to component A by a 180° rotation about the [100] axis in direct or reciprocal space. The twinning matrix for this operation is [1 0 −0.15, 0 −1 0, 0 0 −1]. Laue crystal symmetry system constraints were used during data integration, and the cell parameters and orientation matrix were refined and updated every 100 frames. All final parameters were generated from the refinement of the *xyz* centroids of 2405 strong reflections with $I > 10\sigma$. The intensities were corrected for beam inhomogeneity, absorption, and decay by application of the program SADABS.[11] The transmission factors are between 0.71 and 1.00. Of the 37 705 unique reflections, a total of 7774 with $I > 2\sigma(I)$ and $R_{int} = 0.1642$ remained after data reduction. The structure was solved and refined with the SHELXTL 5.10 package. The positions of all non-hydrogen atoms were located by direct methods and refined anisotropically by full-matrix least squares on F^2. Hydrogen atoms were placed in idealized positions. The final refinement was based on 7774 unique reflections and 325 parameters to give R1 = 0.0642 and wR2 = 0.1396 ($I > 2\sigma$). The goodness-of-fit was 0.910, and the highest peak in the final difference map was 0.663 $e^-/Å^3$

IV. Results and Discussion

A. Syntheses of [M$_2$Cl$_6$]$^{2-}$ Salts. The salt [H-TMPP]$_2$[Fe$_2$Cl$_6$] was first synthesized in our laboratories from the unexpected reduction of ferric chloride ($FeCl_3$) with the highly basic tertiary phosphine TMPP (TMPP = tris(2,4,6-trimethoxyphenyl)-phosphine).[3a] The purity and yields for this method are not satisfactory; therefore, this compound and a series of related salts were synthesized by the direct reaction of a 1:1 molar ratio of $FeCl_2$ with [A]Cl (A = [H-TMPP]$^+$, [PPh$_4$]$^+$, [Et$_4$N]$^+$, [ppn]$^+$, or [AsPh$_4$]$^+$).[12] This synthetic approach also works for the anhydrous halides $CoCl_2$ and $MnCl_2$ to give salts of [Mn$_2$Cl$_6$]$^{2-}$ and [Co$_2$Cl$_6$]$^{2-}$. The products are hygroscopic, air-sensitive, and easily decompose in coordinating solvents such as CH_3CN and MeOH as illustrated by the formation of [BzNEt$_3$]$_2$[FeCl$_4$] from [BzNEt$_3$]$_2$[Fe$_2$Cl$_6$] in CH_3CN/Et_2O.[12]

The nitrogen donor ligand 2,2′-bipyrimidine (2,2′-bpym) was reacted with A$_2$[Fe$_2$Cl$_6$] (A = PPh$_4$ and Et$_4$N) to investigate the potential of the diferrous salts [Fe$_2$Cl$_6$]$^{2-}$ to undergo adduct formation and to explore the possibility of preparing extended arrays with cooperative magnetic interactions. The [Fe$_2$Cl$_6$]$^{2-}$ core appears to cleave in many of these reactions, however, as evidenced by the isolation and structural determination of Fe$_2$Cl$_4$(2,2′-bpym)$_3$ and [Et$_4$N]Cl·[Fe$_2$Cl$_4$(MeOH)$_4$(μ-2,2′-bpym)] from the reaction of [PPh$_4$]$_2$[Fe$_2$Cl$_6$] and [Et$_4$N]$_2$[Fe$_2$Cl$_6$] with 2,2′-bpym, respectively. Two related compounds, viz., Fe$_2$(NCS)$_4$(2,2′-bpym)$_3$[13a] and Co$_2$(NCS)$_4$(2,2′-bpym)$_3$,[13b] have been recently reported that exhibit antiferromagnetic coupling behavior with J values of −4.1 and −6.2 cm^{-1}, respectively.

B. Molecular Structures. [Fe$_2$Cl$_6$]$^{2-}$ Salts 1−4. ORTEP drawings, selected bond distances, and bond angles are presented in Figures 1−4 and Tables 3−6. The geometry of the [Fe$_2$Cl$_6$]$^{2-}$

(12) Sun, J.-S. Ph.D. Dissertation, Michigan State University, 1994.
(13) (a) Real, A.; Zarembowitch, J.; Kahn, O.; Solans, X. *Inorg. Chem.* **1987**, *26*, 2939. (b) De Munno, G.; Julve, M.; Lloret, F.; Faus, J.; Caneschi, A. *J. Chem. Soc., Dalton Trans.* **1994**, 1175.

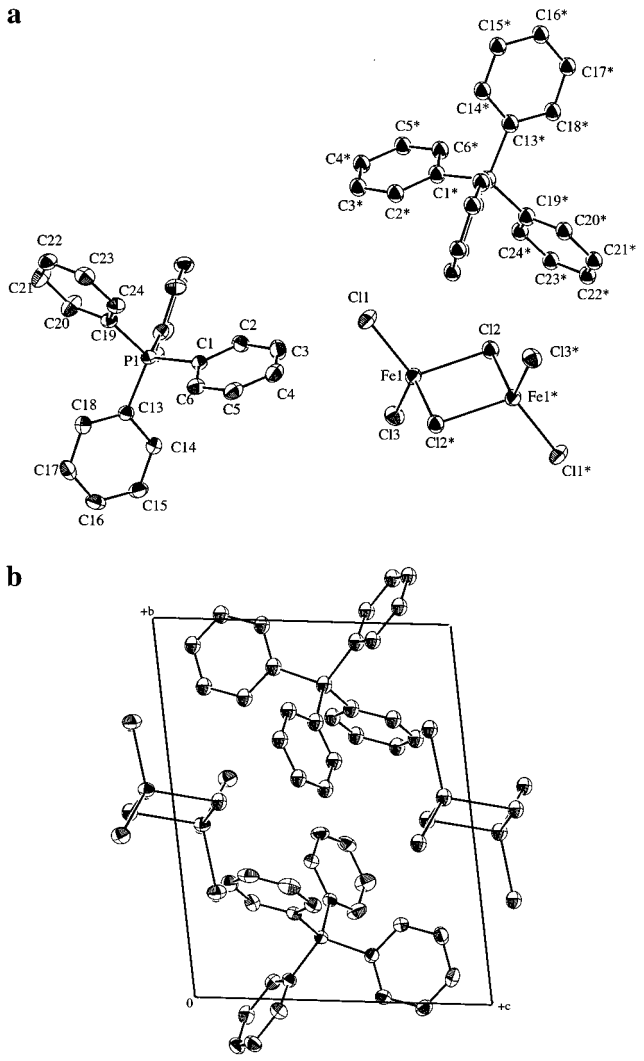

Figure 1. (a) ORTEP representation of $[PPh_4]_2[Fe_2Cl_6]$ (**1**) with thermal ellipsoids at the 50% probability level and (b) packing diagram.

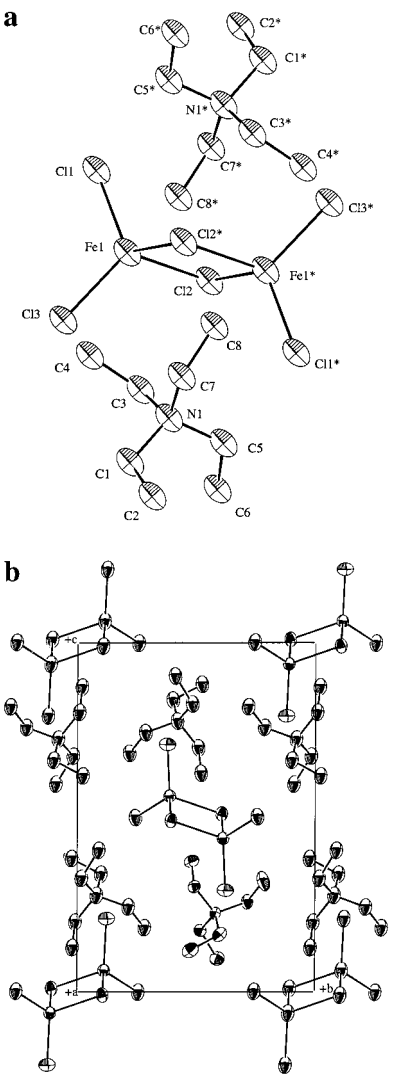

Figure 2. (a) ORTEP representation of $[Et_4N]_2[Fe_2Cl_6]$ (**2**) with thermal ellipsoids at the 50% probability level and (b) packing diagram.

core in all of the salts is of D_{2h} symmetry, which is in accord with the pattern of the stretching vibrations ν(Fe−Cl) (ν_{as}, ν_s, ring) observed in the far-IR region. The average distances of Fe−Cl(terminal) ligands are between 2.235 and 2.265 Å for **1**−**4**, which are similar to distances found in the mononuclear salts $[Fe^{II}Cl_4]^{2-}$ (2.25−2.35 Å)[14] and $[Fe^{III}Cl_4]^{-}$ (2.15−2.20 Å).[15] The bridging angles of Fe−Cl(bridging)−Fe range from 88.64(8)° to 91.8(2)°. In the case of the $[ppn]^+$ salt, it is worth noting that there are two types of $[Fe_2Cl_6]^{2-}$ anions observed in the solid state with different bridging Fe−Cl−Fe angles (91.8(2)° and 88.9(2)°). The anion in $[H\text{-}TMPP]_2[Fe_2Cl_6]$ exhibits the most acute bridging angle, while one of the two types of $[Fe_2Cl_6]^{2-}$ anions in the $[ppn]^+$ salt exhibits the highest obtuse angle. Packing diagrams of **1**−**4** presented in Figures 1−3, respectively, emphasize the orientation of the cations around the $[Fe_2Cl_6]^{2-}$ anions. The shortest contacts between the terminal chlorides of two adjacent $[Fe_2Cl_6]^{2-}$ anions are in the range 5.584(3)−6.642(2) Å. Structural diversity is noted in the way the columns of dimers are arranged, with parallel arrangements observed for **1** and **4**, and zigzag arrangements observed for **2** and **3**.

$[ppn]_2[Co_2Cl_6]$ (6). In the unit cell of this salt, there are two independent $[Co_2Cl_6]^{2-}$ moieties that can be viewed as two edge-sharing bitetrahedra related by an inversion center. The average Co−Cl(terminal) and average Co−Cl(bridging) distances of 2.224(1) and 2.346(1) Å are comparable to the corresponding distances reported in the literature which are in the range 2.212(3)−2.238(6) Å for $Co-Cl_{terminal}$ and 2.329(5)−2.38(3) Å for $Co-Cl_{bridging}$ interactions. The compounds involved in these studies are $[Co[N_6P_6(NMe_2)_{12}]Cl]_2[Co_2Cl_6]\cdot 2CHCl_3$, $[Co_2(\eta^5\text{-}C_5Me_5)_2(\mu_2\text{-}Cl)_3]_2[Co_2Cl_6]$, and $[Co\cdot 15\text{-crown-}5\cdot 2CH_3CN][Co_2Cl_6]$.[16] The Co···Co separation of 3.221(1) Å is shorter than the corresponding values for $[Co_2Cl_6]^{2-}$ reported in the literature, which are in the range 3.277(6)−3.366(3) Å.[17] The Co1−Cl2−Co1* and Cl2−Co−Cl2* angles of 85.79° and 93.29(3)° are

(14) (a) Mason, R.; McKenzie, E. D.; Robertson, G. B.; Rusholme, G. A. *Chem. Commun.* **1968**, 1673. (b) Freeman, H. C.; Milburn, G. H. W.; Nockolds, C. E. *J. Chem. Soc. D* **1969**, 55. (c) Toan, T.; Dahl, L. F. *J. Am. Chem. Soc.* **1971**, *93*, 2654. (d) Lauher, J. W.; Ibers, J. A. *Inorg. Chem.* **1975**, *14*, 348.

(15) (a) Constant, G.; Daran, J.-C.; Jeannin, Y. *J. Organomet. Chem.* **1972**, *44*, 353. (b) Cotton, F. A.; Murillo, C. A. *Inorg. Chem.* **1975**, *14*, 2467. (c) Glowiak, T.; Durcanska, E.; Ondrejkovicova, I.; Ondrejovic, G. *Acta Crystallogr.* **1986**, *C42*, 1331. (d) Walker, J. D.; Poli, R. *Polyhedron* **1989**, *8*, 1293. (e) Cotton, F. A.; Luck, R. L.; Son, K.-A. *Acta Crystallogr.* **1990**, *C46*, 1424 and references therein.

(16) (a) Harrison, W.; Trotter, J. *J. Chem. Soc., Dalton Trans.* **1973**, 61. (b) Olson, W. L.; Dahl, L. F. *Acta Crystallogr.* **1986**, *C42*, 541. (c) Kireeva, O. K.; Bulychev, B. M.; Streltsova, N. R.; Belsky, V. K.; Dunin, A. G. *Polyhedron* **1992**, *11*, 1801.

(17) (a) Saak, W.; Haase, D.; Pohl, S. *Z. Naturforsch.* **1988**, *43B*, 289. (b) Ruhlandt-Senge, K.; Müller, U. *Z. Naturforsch.* **1992**, *47B*, 1075.

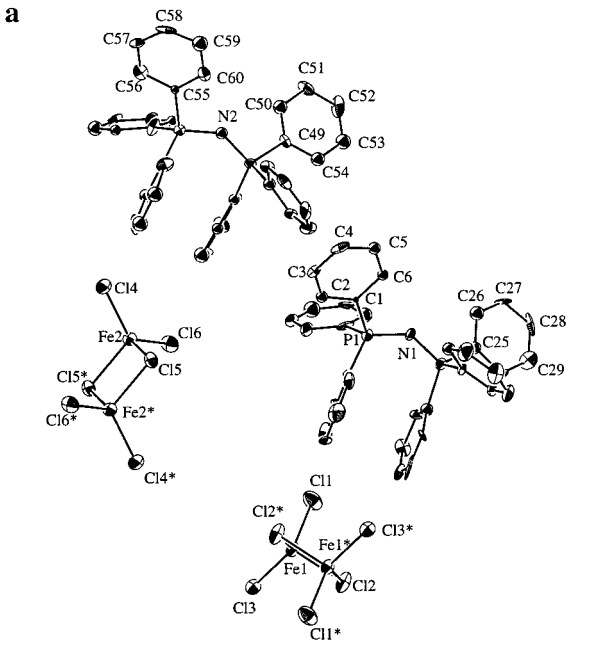

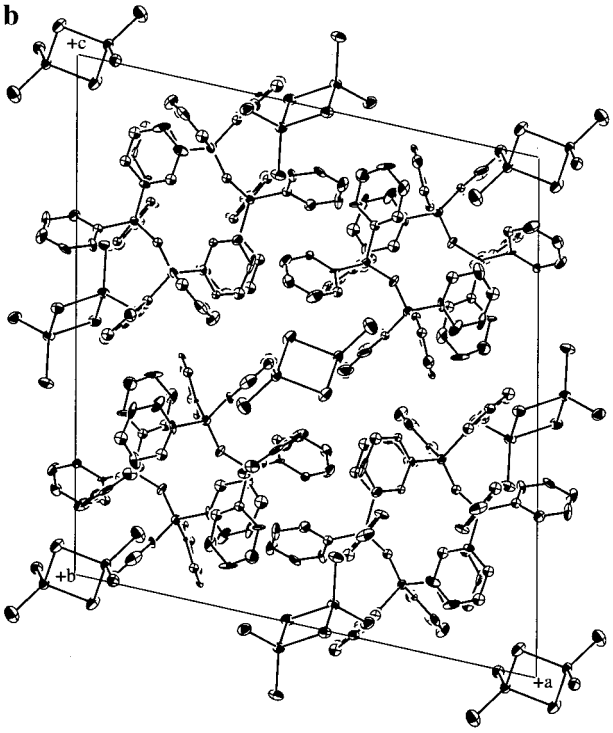

Figure 3. (a) ORTEP representation of $[ppn]_2[Fe_2Cl_6]$ (**3**) with thermal ellipsoids at the 50% probability level and (b) packing diagram.

considerably distorted from an ideal tetrahedral geometry due to the formation of the four-membered ring. Both of the $[Co_2Cl_6]^{2-}$ units exhibit Cl−Co−Cl angles larger than 90°, in contrast to the $[ppn]_2Fe_2Cl_6$ structure, in which one of the anions exhibits an angle less than 90°. Among the members of the $[ppn]_2M_2Cl_6$ series the *intramolecular* Co···Co separation in **6** is the shortest, and the Co−Cl−Co angle is the smallest (Table 11). The shortest *intermolecular* contact between the anions (Cl···Cl) is 5.555(1) Å. Selected bond distances and angles are listed in Table 7. A projection diagram viewed down the *b* axis in Figure 5 illustrates the arrangement of the $[ppn]^+$ cations and the $[Co_2Cl_6]^{2-}$ anions in the unit cell.

$[ppn]_2[Mn_2Cl_6]$ (7). The $[ppn]_2[Mn_2Cl_6]$ structure is similar to the Co analogue, with two independent dimetal anions occupying the asymmetric unit, and the Cl−Mn−Cl angle being greater than 90°. The average Mn−Cl(terminal) and average Mn−Cl(bridging) distances of 2.309(1) and 2.446(1) Å are comparable to corresponding distances reported in the literature (2.306(2) Å for distances of $Mn-Cl_{terminal}$ and 2.440(2) Å for distances for $Mn-Cl_{bridging}$).[18] Likewise, the average Mn···Mn separation of 3.376(1) Å is similar to analogous distances found in other compounds.[18] The average Mn1−Cl2−Mn1* and Cl2−Mn−Cl2* angles of 87.25(2)° and 92.75(2)° are considerably distorted from an ideal tetrahedral geometry. A projection diagram viewed down the *b* axis in Figure 6a illustrates the arrangement of the $[ppn]^+$ and the $[Mn_2Cl_6]^{2-}$ anions in the unit cell. The closest *intermolecular* interaction between anions is 5.720(1) Å. Selected *intramolecular* bond distances and angles are listed in Table 8.

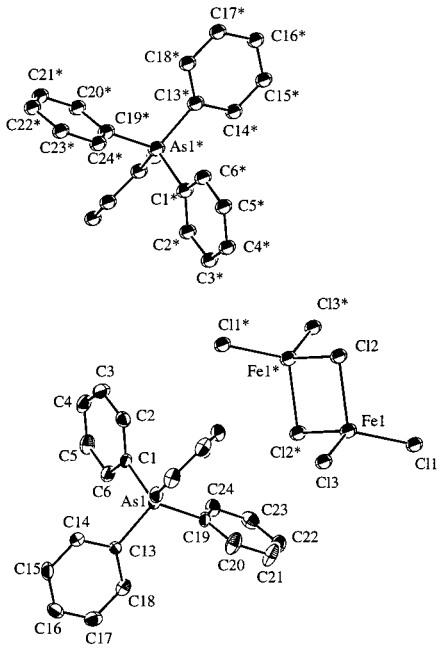

Figure 4. ORTEP representation of $[AsPh_4]_2[Fe_2Cl_6]$ (**4**) at the 50% probability level. The packing arrangement is identical to that of **1**.

$Fe_2Cl_4(2,2'\text{-bpym})_3$ (8). This neutral complex consists of Fe(II) dimeric units bridged by a 2,2′-bpym ligand acting as a bis-chelating ligand. In contrast to the previous compounds in which the metal is tetrahedral, the Fe(II) centers are in an octahedral environment. An ORTEP drawing and selected bond distances and bond angles for $Fe_2Cl_4(2,2'\text{-bpym})_3$ are presented in Figure 7 and Table 9. The average Fe−Cl bond distance is 2.40 Å, which is longer than the corresponding distances reported for $Fe^{II}-Cl$ in $[FeCl_4]^{2-}$ (2.25−2.35 Å)[14] and $Fe^{III}-Cl$ in $[FeCl_4]^-$ (2.15−2.20 Å).[15] The Fe−N(terminal) bond distances are 2.208(3) and 2.187(3) Å, which are similar to those reported for $Fe_2(NCS)_4(2,2'\text{-bpym})_3$ (2.200(6) and 2.211(6) Å)[13a] but shorter than the Co−N distances in $Co_2(NCS)_4(2,2'\text{-bpym})_3$ (2.161(2) and 2.127(2) Å).[13b] The $Fe-N_{bridging}$ bond distances of 2.224(3) and 2.271(3) Å are shorter than those reported for $Fe_2(NSC)_4(2,2'\text{-bpym})_3$ (2.316(6) Å) but are essentially the same as the $Co-N_{bridging}$ distances in $Co_2(NCS)_4(2,2'\text{-bpym})_3$, which are 2.185(2) and 2.279(2) Å. The *intramolecular* Fe···Fe separation is 5.918(2) Å, which is much longer than the corresponding distance of 5.522(6) Å in $Fe_2(NCS)_4(2,2'\text{-bpym})_3$.

(18) (a) Pampaloni, G.; Englert, U. *Inorg. Chim. Acta* **1995**, *231*, 167. (b) Brass, C.; Robert, R.; Bachet, B.; Chevalier, R. *Acta Crystallogr., Sect. B* **1976**, *32*, 1371. (c) Goodyear, J.; Ali, E. M.; Shutherland, H. H. *Acta Crystallogr., Sect. B* **1978**, *34*, 2617.

Table 11. Metrical Parameters for the $[M_2Cl_6]^{2-}$ Anions[a]

compd	M−Cl_b−M	M−M (intra)	Cl_t−M−Cl_b	Cl_t−M−Cl_t
(M = Fe, **1**)	91.79(3)	3.4517(9)	110.01(3)	118.86(3)
			112.16(3)	
			110.95(3)	
			112.49(4)	
(M = Fe, **2**)	91.12(3)	3.4232(9)	110.53(4)	116.74(4)
			112.33(3)	
			113.27(3)	
			111.83(3)	
(M = Fe, **3**)	91.8(2)	3.452(6)	109.5(2)	120.0(2)
			110.4(2)	
			110.7(2)	
			113.5(2)	
	88.9(2)	3.353(6)	105.3(2)	119.82(2)
			114.5(2)	
			115.5(2)	
			107.2(2)	
(M = Fe, **4**)	91.12(4)	3.431(1)	109.28(5)	119.52(5)
			112.25(5)	
			110.48(5)	
			112.17(5)	
(M = Fe, **5**)	88.64(8)	3.350(4)	108.02(9)	120.5(1)
			110.57(8)	
			110.96(9)	
			111.50(8)	
(M = Co, **6**)	85.79(3)	3.191(1)	114.81(2)	115.94(4)
			106.86(4)	
			114.34(4)	
			108.76(4)	
	87.63(3)	3.251(1)	109.94(5)	115.57(4)
			112.34(4)	
			113.55(4)	
			110.75(5)	
(M = Mn, **7**)	86.37(2)	3.344(1)	105.58(3)	118.00(3)
			113.82(3)	
			114.49(3)	
			108.79(3)	
	88.13(2)	3.408(1)	108.63(3)	118.21(3)
			110.04(3)	
			111.52(3)	
			113.40(3)	

[a] Cl_t: terminal chloride. Cl_b: bridging chloride.

A 2-D projection view of $Fe_2Cl_4(2,2'\text{-bpym})_3$ viewed down the *b* axis is presented in Figure 7b. The closest *intermolecular* Fe···Fe contact of 7.047(1) Å is much shorter than the corresponding distance reported for $Fe_2(NCS)_4(2,2'\text{-bpym})_3$ (9.138(2) Å) as a result of the π-stacking of the 2,2′-bpym ligands. The fact that the thiocyanate derivative does not exhibit close contacts between bipyrimidine rings may be rationalized by the fact that the smaller ligand Cl^- allows for a closer separation between two molecules than does the larger SCN^- ligand.

$[Et_4N]Cl\cdot[Fe_2Cl_4(MeOH)_4(\mu\text{-}2,2'\text{-bpym})]$ (9). Cleavage of the $[Fe_2Cl_6]^{2-}$ core was also observed to occur in the reaction between $[Et_4N]_2[Fe_2Cl_6]$ and 2,2′-bipyrimidine in MeOH. The compound $[Et_4N]Cl\cdot Fe_2Cl_4(MeOH)_4(\mu\text{-}2,2'\text{-bpym})$ consists of two Fe(II) atoms united by a bis-chelating 2,2′-bpym ligand and further bonded to two terminal chloride and two methanol ligands. An ORTEP drawing as well as selected bond distances and bond angles are presented in Figure 8 and Table 10. Interestingly, the unit cell also contains 1 equiv of $[Et_4N]Cl$ that serves to fill void space as well as to assist in connecting the neutral, dinuclear molecules into an infinite chain via hydrogen bonds between the outer-sphere Cl^- ions and the axial MeOH ligands. The average hydrogen-bonding distance between the Cl^- ions and the axial methanols is 2.315(7) Å. The average Fe−Cl bond distance is 2.383(2) Å. The 2,2′-bpym ring is tilted slightly out of the plane containing the Fe centers by ~0.0149 Å.

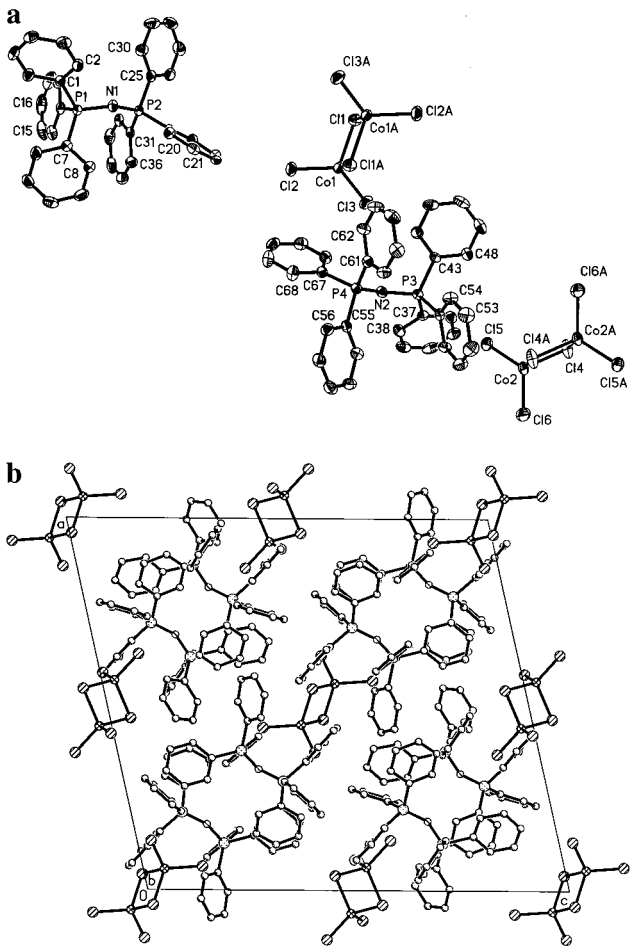

Figure 5. (a) ORTEP representation of the $[Co_2Cl_6]^{2-}$ anion in $[ppn]_2[Co_2Cl_6]$ (**6**) at the 50% probability level and (b) 2-D projection looking down the *b* direction.

The Fe1−$N_{bridging}$ bond distances of 2.224(6) and 2.239(6) Å differ slightly from the Fe2−$N_{bridging}$ bond distances of 2.244(6) and 2.250(6) Å. The separation between two *intramolecular* Fe(II) atoms is 5.957 Å, and the closest *intermolecular* Fe···Fe contact is 7.964 Å, which is much longer than the corresponding distance of 7.047(1) Å in $Fe_2Cl_4(2,2'\text{-bpym})_3$.

C. Magnetic Studies. Since one of the main goals of this work is to use $[Fe_2Cl_6]^{2-}$ as a source of the diferrous ion in reactions with polydentate ligands, we undertook a comprehensive study of the magnetic properties of various salts of this anion and of analogous $[M_2Cl_6]^{2-}$ anions with M = Co(II) and Mn(II). Four complexes containing the $[Co_2Cl_6]^{2-}$ moiety,[16] and $[M_2X_6]^{2-}$ salts containing various metals and halides such as $[Fe_2I_6]^{2-}$ and $[Mn_2X_6]^{2-}$ (X = Cl, Br, I) have appeared in the literature,[17−19] but no magnetic studies of these compounds accompanied these reports. For the Fe compounds, salts containing four different counterions were studied to probe the effect of cation size and packing influences on the magnetic interactions of the compounds.

Magnetic Properties of $[Fe_2Cl_6]^{2-}$ Salts. These compounds are very air sensitive; therefore, all manipulations were performed in a drybox, where the polycrystalline samples were introduced into a holder that consists of an inert polymer folded into a very small packet. In order to check the reproducibility of the magnetic results on these air-sensitive materials, the magnetic measurements were carried out for at least two

(19) Pohl, S.; Saak, W.; Stolz, P. *Z. Naturforsch.* **1988**, *43B*, 171.

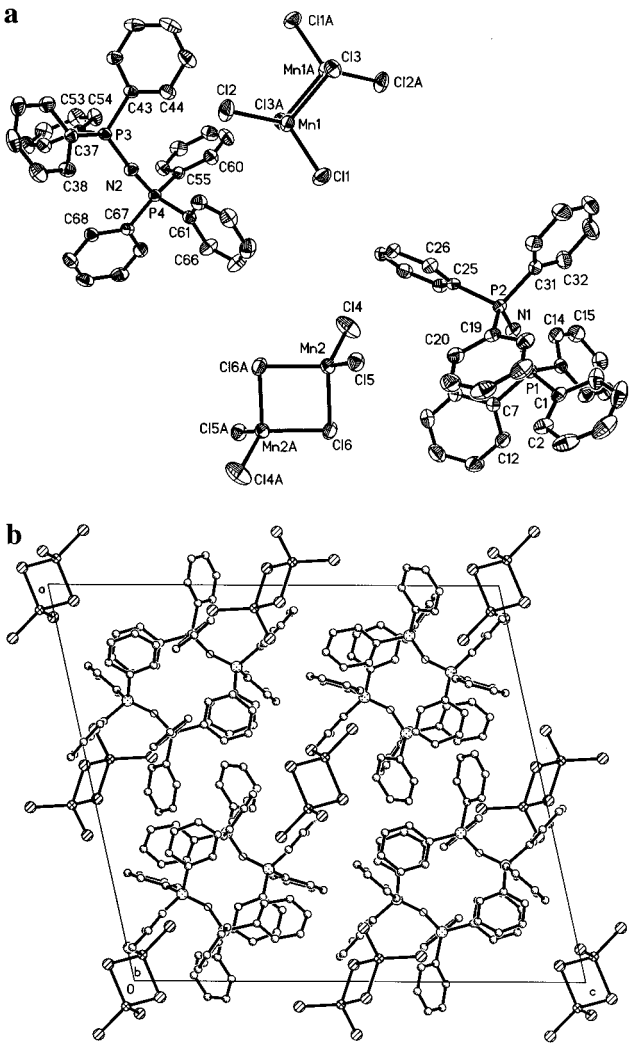

Figure 6. (a) ORTEP representation of the $[Mn_2Cl_6]^{2-}$ anion in $[ppn]_2[Mn_2Cl_6]$ (**7**) at the 50% probability level and (b) 2-D projection looking down the *b* axis.

independent batches. The observed behavior was always reproducible. The χT curves do not change from sample to sample, although changes in the susceptibility values up to 10% can be observed that may be attributed to small amounts of ferric impurities (few percent) or to uncertainties in the correction of the holder at high temperatures.

The magnetic data of **1**−**5** are summarized in Figure 9. In all cases, χT shows a decrease at low temperatures (below 20−30 K) which suggests the presence of antiferromagnetic exchange coupling between the metal ions, although the local anisotropy of Fe^{II} is also important. In distorted tetrahedral environments, this ion typically exhibits values for the zero-field-splitting parameter, *D*, in the range 5−10 cm^{-1}, which is quite large.[1b,g] The appropriate spin Hamiltonian for this type of dinuclear compound is written as

$$\hat{H}_0 = -2J\hat{\mathbf{S}}_1\hat{\mathbf{S}}_2 + D(\hat{S}_{z1}^2 + \hat{S}_{z2}^2) \qquad (1)$$

In this equation, $\mathbf{S}_1$ and $\mathbf{S}_2$ are the spin operators associated with the ground state of the tetrahedral Fe^{II} ions, ^5E, which is well-described as a spin-only with $S = 2$; S_{1z} and S_{2z} are their *z* components, and *J* and *D* are the exchange and ZFS parameters, respectively. A Zeeman term must be added to the above Hamiltonian to analyze the magnetic properties. In view of the spin anisotropy produced by the ZFS term, this Hamiltonian should consider both parallel and perpendicular *g* components:

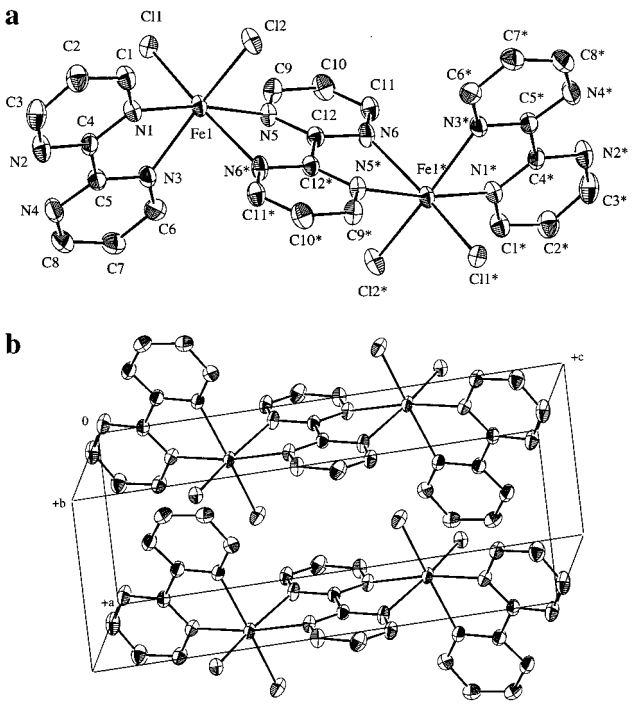

Figure 7. (a) ORTEP representation of $Fe_2Cl_4(bpym)_3$ (**8**) at the 50% probability level and (b) packing diagram.

$$\hat{H}_{Zee} = \beta\sum_{1,2}(g_{||i}H_z\hat{S}_{zi} + g_{\perp i}(H_x\hat{S}_{xi} + H_y\hat{S}_{yi})) \qquad (2)$$

The full Hamiltonian is being solved by a numerical procedure based on a program recently developed by us that allows one to calculate the magnetic properties (susceptibility, magnetization) of magnetic clusters of arbitrary nuclearity and topology described by a general spin Hamiltonian that considers both isotropic and anisotropic terms.[20] To fit the powder susceptibility data is not a trivial feat, as both antiferromagnetic *J* and positive *D* produce the same effect in the magnetic behavior, i.e., a decrease of χT at lower temperatures or a stabilization of a nonmagnetic ground spin state. Therefore, to obtain reliable information on these two parameters, the magnetic susceptibility data were complemented by a fitting of the magnetization data. The fitting procedure involves a self-consistent method: In the first step various solutions that closely reproduce the susceptibility data are obtained. In a second step various sets of parameters are examined to determine which one better reproduces the magnetization data. In a final step this set is refined in order to simultaneously optimize the fit of both kinds of experimental measurements. As a result of this third step an anisotropic *g* is required in some cases. It is to be noted that, when such anisotropy is neglected, reasonable fits are also obtained, although the agreement factor is slightly worse. In any case the fact of taking or not taking into account the anisotropy in *g* does not affect the *J* and *D* values within the experimental error. Therefore, we have preferred to provide the set of parameters that represent the best fits to the experimental data (Table 12). It must be emphasized that the magnetic susceptibility fit is not very sensitive to the relative values of *J* and *D*. Nevertheless, a careful study of the quantitative effect of these two parameters

(20) (a) Clemente-Juan, J. M. Doctoral Dissertation, University of Valencia, 1998. (b) Borrás-Almenar, J. J.; Clemente-Juan, J. M.; Coronado, E.; Tsukerblat, B. *Inorg. Chem.*, in press.

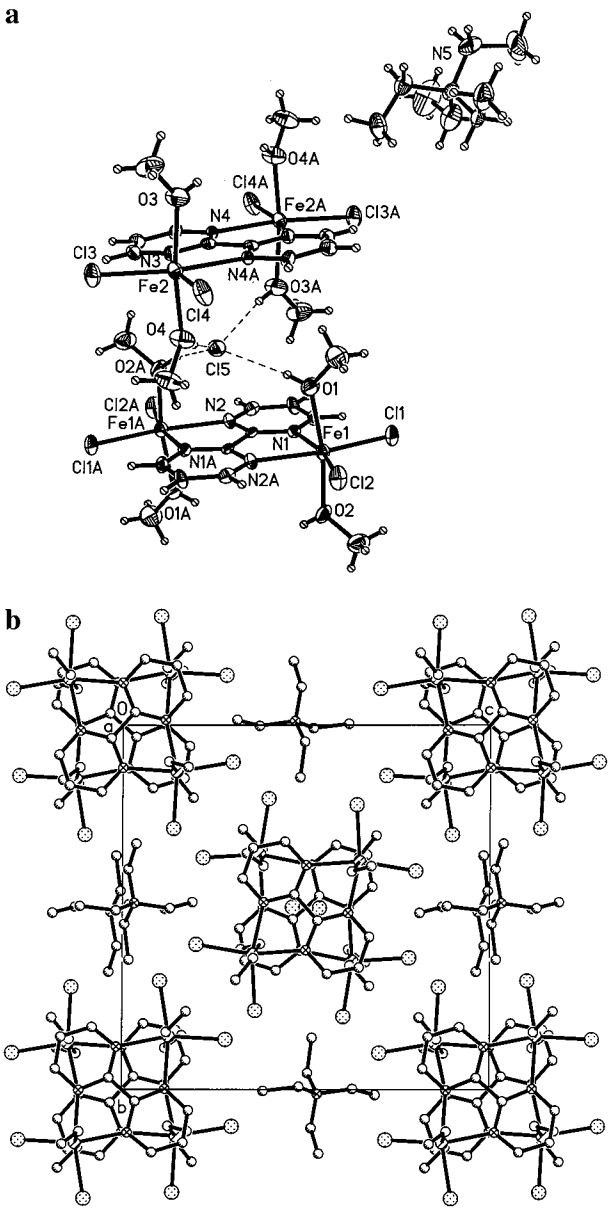

Figure 8. (a) ORTEP representation of $[Et_4N]Cl{\cdot}[Fe_2Cl_4(MeOH)_4(\mu\text{-}2,2'\text{-bpym})]$ (**9**) at the 40% probability level and (b) packing diagram.

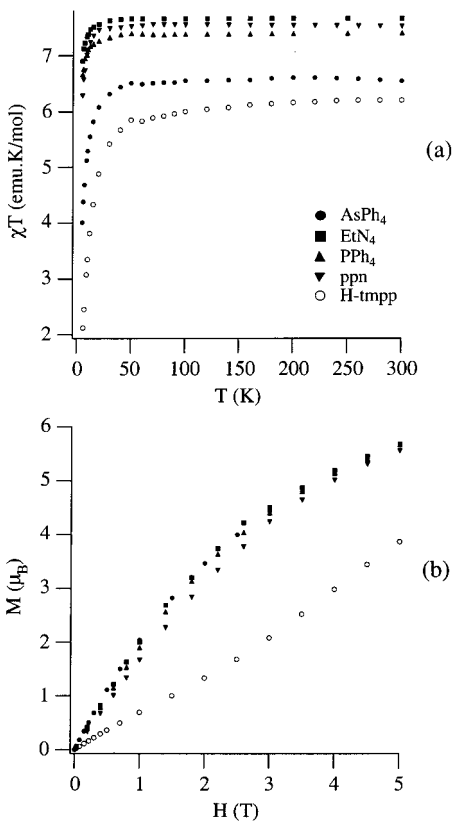

Figure 9. Magnetic properties of the various $[Fe_2Cl_6]^{2-}$ salts: (a) thermal dependence of the product χT; (b) magnetization curves at 5 K.

Table 12. Magnetic Parameters for the $[M_2Cl_6]^{2-}$ Anions

compd	J (cm^{-1})	D (cm^{-1})	g
$[PPh_4]_2[Fe_2Cl_6]$ (**1**)	0.07 (∼0)	4.9	$g_\perp = 2.20$, $g_\parallel = 2.25$
$[Et_4N]_2[Fe_2Cl_6]$ (**2**)	0.10 (∼0)	5.2	$g_\perp = 2.23$, $g_\parallel = 2.31$
$[ppn]_2[Fe_2Cl_6]$ (**3**)	0.07 (∼0)	6.3	2.24
$[AsPh_4]_2[Fe_2Cl_6]$ (**4**)	−0.05 (∼0)	4.5	$g_\perp = 2.00$, $g_\parallel = 2.30$
$[H\text{-}TMPP]_2[Fe_2Cl_6]$ (**5**)	−0.74	3.7	$g_\perp = 2.00$, $g_\parallel = 2.20$
$[ppn]_2[Co_2Cl_6]$ (**6**)	−11.6	29.0	2.25
$[ppn]_2[Mn_2Cl_6]$ (**7**)	15.6, −0.69		2.05

revealed important differences. In fact, antiferromagnetic coupling alone was largely unable to reproduce the low-temperature magnetic behavior. The magnetic behavior is reproduced much better when the ZFS parameter is the leading contributor. Thus, in four of the five salts that were measured, viz., $[PPh_4]^+$ (**1**), $[Et_4N]^+$ (**2**), $[ppn]^+$ (**3**), and $[AsPh_4]^+$ (**4**), the exchange coupling was found to be close to zero, while D was between 4.5 and 6.3 cm^{-1}. The only case in which antiferromagnetic coupling was required to fit the data is the $[H\text{-}TMPP]^+$ derivative (**5**) (Figure 10). In this compound, the decrease in χT is much more important than in the other three cases so that a ratio $|J|/D = 0.20$ was obtained with a D value of 3.5 cm^{-1}.

The above difference is confirmed by the low-temperature magnetization data, which is much more sensitive to the $|J|/D$ ratio. Thus, while in compounds **1**−**4** the curvature of M versus H is negative over the whole range from 0 to 5 T as expected for a dominant ZFS parameter, the curvature is positive in **5**, supporting the presence of a non-negligible antiferromagnetic exchange. The quantitative validity of this last result is reflected in the good fits of these magnetization data (solid line in Figure 10b). A better estimate of D can be obtained from the analysis of the thermal dependence of the magnetization at various fixed magnetic fields (2, 4, and 5 T). These curves are plotted for one of the compounds having a negligible exchange coupling **3** and for **5** (Figure 11a and b). Although the fit is not perfect, these data permit us to assess the errors affecting the D values. For example, as illustrated in Figure 11, the D value for $[ppn]_2[Fe_2Cl_6]$ (**3**) is within the range 5−7 cm^{-1}, while for $[H\text{-}TMPP]_2[Fe_2Cl_6]$ (**5**) it is within the range 3−4 cm^{-1}. The small differences between theory and experiment can be due to other effects not considered by the model, as for example the influence of a rhombic component in the ZFS (E parameter). An additional source of error can arise from the magnetization measurements themselves. Since these measurements are performed at low temperatures, they are affected to a larger extent than the magnetic susceptibility data by contributions from paramagnetic impurities.

In summary, a combination of magnetic susceptibility and magnetization measurements have shown that the most important parameter in the $[Fe_2Cl_6]^{2-}$ anions is D. The exchange parameter is small; thus it is difficult to obtain reliable values for J, except in the case of **5**, for which the magnetic susceptibility data indicate that the exchange is antiferromag-

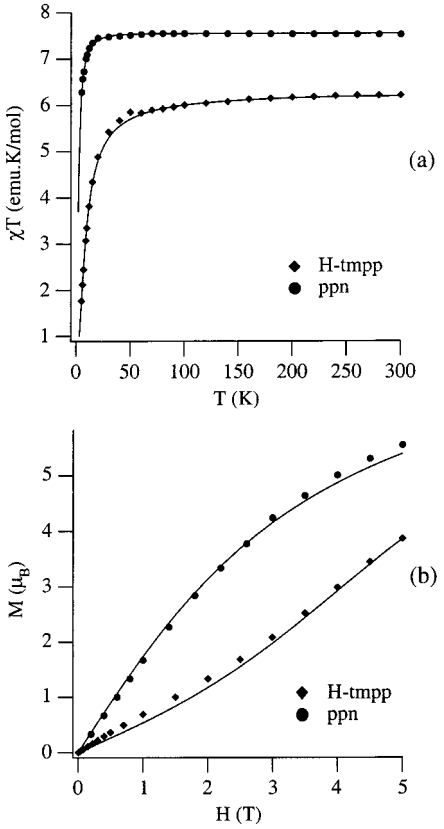

Figure 10. Magnetic properties of the (a) **3** and (b) **5** salts. The solid lines represent the best fit to the anisotropic model (see eq 1) using the parameters from Table 12.

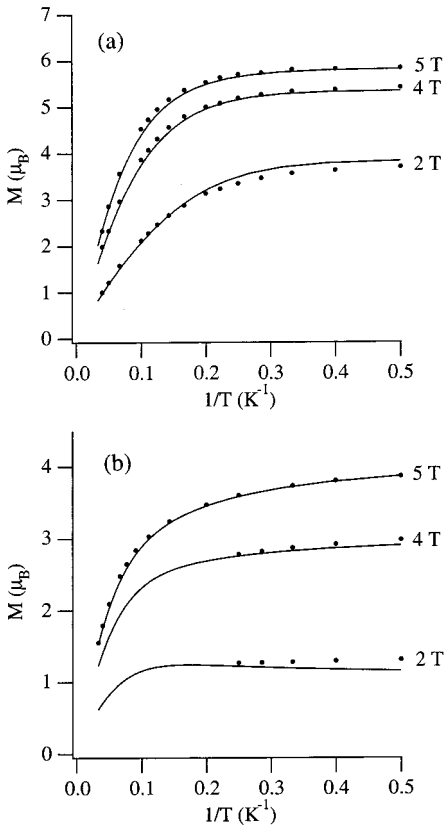

Figure 11. Magnetization curve vs T^{-1} (a) for **3** and (b) for **5** at different fields (filled circles). Comparison with the theory (solid line) using the parameters from Table 12.

netic. In the other four compounds, the ratio $|J|/D$ is so small that even the sign of the exchange is not definitive. The magnetic differences between the $[H\text{-}TMPP]^+$ derivative and the other compounds may be correlated to structural differences within the dimer. In fact, the Fe−Cl−Fe angle in **5** is the most acute one of the series (88.9°) (Table 11), and the *intermolecular* anion distance is slightly shorter by 0.1 Å. This favors greater overlap between the magnetic orbitals, resulting in a larger value of the antiferromagnetic contribution to the exchange.

Magnetic Properties of $[ppn]_2[Co_2Cl_6]$ and $[ppn]_2[Mn_2Cl_6]$. The magnetic properties of the $[ppn]^+$ salt of Co(II) are depicted in Figure 12, which contains plots of χ vs T and χT vs T. These data suggest the presence of strong antiferromagnetic exchange interactions between the Co(II) ions. A rounded maximum in χ at 50 K is observed, while χT reveals a continuous decrease from a value of 4.22 emu K/mol at 300 K to a value close to zero at 2 K. In tetrahedral environments, Co(II) is described by a $^4A_2$ term. Therefore, the Hamiltonian in eq 1 was expected to be appropriate to describe its properties, as it contains an isotropic exchange term supplemented by a zero-field splitting term to account for the single-ion anisotropy of the spin $S = {}^3/_2$ of Co(II). In an initial fitting exercise, we attempted to reproduce the magnetic properties by a fully isotropic Hamiltonian, i.e., by neglecting the single-ion anisotropy contribution. This simple model completely failed to fit the magnetic data. In particular, significant differences between theory and experiment were observed in the region near the maximum in χ (dotted line in Figure 12). In a second fitting, the ZFS term was taken into account, which introduces magnetic anisotropy. In a manner similar to the treatment of the Fe compounds, the model calculates the two components of the magnetic susceptibility ($\chi_{\parallel}$ and $\chi_{\perp}$) in order to obtain the theoretical curve for a powder ($\chi_{powder} = (\chi_{\parallel} + 2\chi_{\perp})/3$). With this additional term the magnetic behavior is closely reproduced in the whole temperature range for $J = -11.6$ cm^{-1}, $D = 29.0$ cm^{-1}, and $g = 2.25$ (solid line in Figure 12). A small amount of an $S = {}^3/_2$ paramagnetic impurity (0.16%) was introduced to reproduce the Curie tail observed below 4 K.

In summary, the spin anisotropy is again the dominant contribution (the ratio $|J|/D$ is equal to 0.4), although a stronger antiferromagnetic coupling is present. This large D value correlates well with the structural features which indicate a much greater distortion of the tetrahedral site than is present in the Fe analogues. The acute Co−Cl−Co angles (85.79(3)° and 87.63(3)°) taken together with the short Co−Co separation can account for the presence of appreciable antiferromagnetic coupling.

Plots of the magnetic data for $[ppn]_2[Mn_2Cl_6]$ are provided in Figure 13. A continuous decrease in χT is observed upon cooling, which is indicative of dominant antiferromagnetic interactions. In this case, the ZFS is expected to be quite small compared to J, as the ground state of Mn(II) is described by a $^6A_1$ term. Thus, a fully isotropic Heisenberg Hamiltonian should be suitable for describing the properties. As one can clearly see from the data, however, this model does not satisfactorily reproduce the experimental behavior (dotted line in Figure 13). A model assuming two antiferromagnetic J parameters of different magnitudes was used to improve this fit. The consideration of a second exchange coupling in this system may be due to the presence of a weak antiferromagnetic coupling between molecules. A simple model that accounts for this effect is that of an alternating $J-J'$ chain of spins $^5/_2$. If these spins are treated as classical, an analytical expression can be

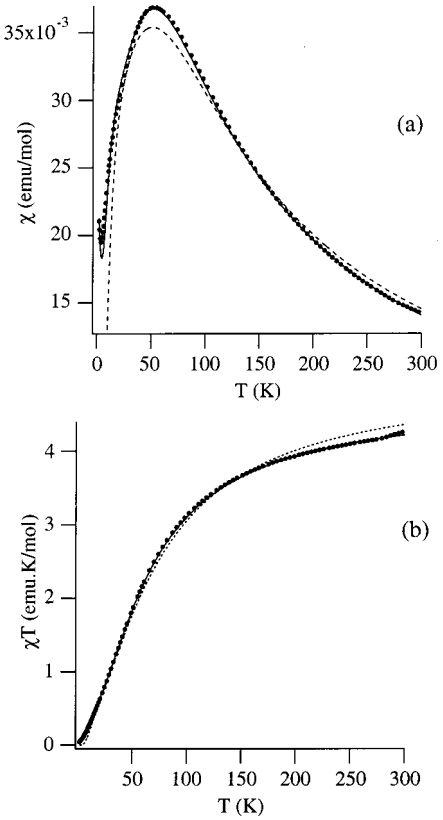

Figure 12. Thermal dependence of the (a) susceptibility and of the (b) product χT for $[ppn]_2[Co_2Cl_6]$. The best fit to the anisotropic model is shown as a solid line. The theoretical behavior of a fully isotropic antiferromagnetic Co(II) dimer is shown as a dotted line.

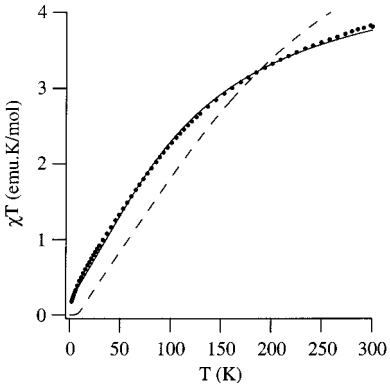

Figure 13. Thermal dependence of the product χT for $[ppn]_2[Mn_2Cl_6]$ (filled circles) and the best fit to a two-exchange dimeric model (solid line). The theoretical behavior of an antiferromagnetic Mn(II) dimer is shown as a dotted line.

obtained.[21] Using this expression, a good fit of the experimental data was obtained. The best fit, shown as a solid line in Figure 13, corresponds to the parameter values of $J = -15.6$ cm^{-1}, $J' = -0.69$ cm^{-1}, and $g = 2.05$. In order to reproduce the data, a paramagnetic $S = {}^5/_2$ impurity of 3% was introduced.

Magnetic Properties of the Bipyrimidine Compounds. Our recent discovery that the diferrous anion $[Fe_2Cl_6]^{2-}$ can be prepared from reactions of anhydrous $FeCl_2$ with 1 equiv of Cl^- ion has provided entry into a new building block for magnetic compounds. Compounds containing the 2,2′-bipyrimidine ligand bridging two transition metal ions are of considerable interest due to their intriguing electronic and magnetic properties.[4] Bipyrimidine is of particular interest because it can act as a bis-chelating ligand toward transition metal ions and transmit magnetic interactions.

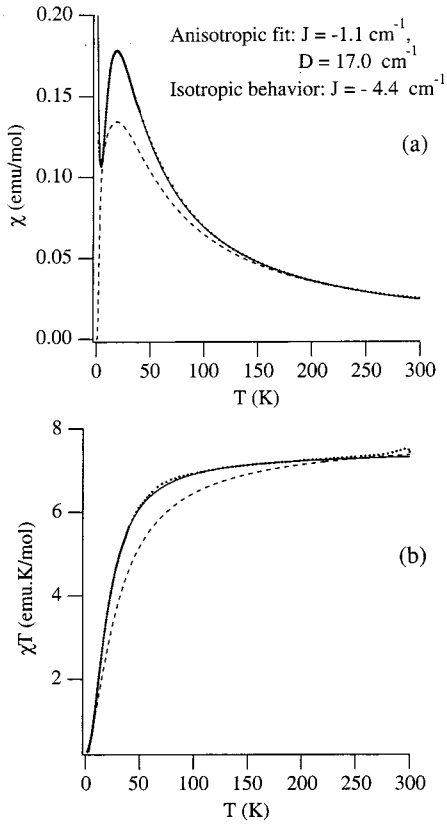

Figure 14. Thermal dependence of the (a) susceptibility and of (b) the product χT for $Fe_2Cl_4(2,2'\text{-bpym})_3$. Dotted lines are the theoretical behaviors of fully isotropic antiferromagnetic dimers. The best fit to the anisotropic model is shown as a solid line.

Plots of χ and χT versus temperature for $Fe_2Cl_4(2,2'\text{-bpym})_3$ are presented in Figure 14. The molar magnetic susceptibility reaches a maximum at 20 K. At low temperatures, below 10 K, a Curie tail is observed that is associated with a small amount of $S = 2$ paramagnetic impurity. The curve of χT versus temperature decreases continuously upon cooling and approaches zero as the temperature approaches absolute zero. These features agree with the presence of antiferromagnetically coupled paramagnetic centers. In order to fit these data we have again used the spin Hamiltonian in eq 1. It is important to point out, however, that the present case is different from the $[Fe_2Cl_6]^{2-}$ anion reported in this paper, since the metal environment is octahedral instead of tetrahedral. The electronic ground state of Fe(II) in $Fe_2Cl_4(2,2'\text{-bpym})_3$ is an orbitally degenerate one, $^4T_1$. The study of the exchange phenomenon in the presence of orbital degeneracy is an open problem in magnetism for which no general solution is available.[22] In order to treat the present system we have assumed that the simple spin Hamiltonian defined in eq 1 is still valid, as the role of the orbital contribution is to introduce a strong magnetic anisotropy in the system. Thus, a comparatively large single-ion anisotropy should account for this effect, as it results in an effective exchange anisotropy.[23] In fact, an isotropic exchange alone is completely unable to reproduce the magnetic data. As can be observed in

(21) Cortés, R.; Drillon, M.; Solans, X.; Lezama, L.; Rojo, T. *Inorg. Chem.* **1997**, *36*, 677.

(22) Borrás-Almenar, J. J.; Clemente-Juan, J. M.; Coronado, E.; Palii, A. V.; Tsukerblat, B. S. *J. Phys. Chem. A* **1998**, *102*, 200.

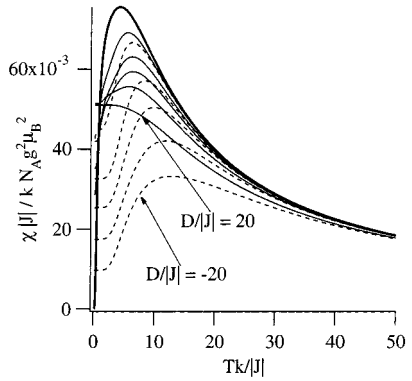

Figure 15. Anisotropic model for an antiferromagnetic dinuclear complex of spins $S = 2$ showing the influence of the sign and magnitude of the single-ion anisotropy parameter, D.

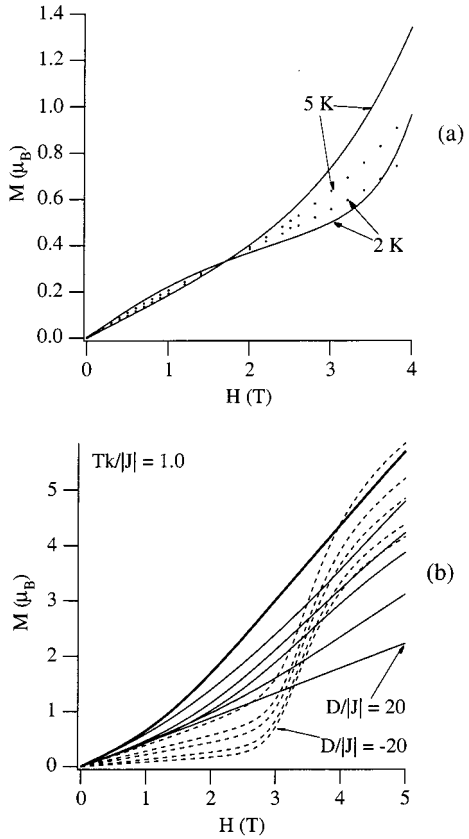

Figure 16. (a) Isothermal magnetizations at 2 and 5 K for $Fe_2Cl_4(2,2'\text{-bpym})_3$. Solid lines are the theoretical behaviors calculated using the anisotropic model results. (b) Influence of the single-ion anisotropy parameter, D, on the isothermal magnetization.

Figure 14a (dotted lines), if one tries to reproduce the position of the maximum in χ, its height is significantly below the experimental magnetic data, while if one attempts to reproduce the shape, the calculated maximum is located significantly above the experimental one and at lower temperatures. When spin anisotropy is taken into account, however, these problems can be eliminated. In particular, the influence of a negative D is to decrease the maximum χ value and to shift it to higher temperatures (Figure 15). Conversely, when D is positive and large compared to J, the maximum in χ tends to disappear. Accordingly, in order to fit the magnetic data, a large and negative D value is necessary. The final set of parameters that were used for the best fit are $J = -1.1 \pm 0.1$ cm^{-1}, $D = -17.0 \pm 2$ cm^{-1}, and $g = 2.24$. The amount of $S = 2$ paramagnetic impurity is 3.1%. The agreement is excellent in the overall temperature range (solid lines in Figure 14). A definitive proof of the validity of these parameters, and in particular of the sign of D, can be obtained from the analysis of the low-temperature magnetization data (Figure 16a). Although the fit is not exact, the most significant features are reproduced by the model. Thus, the experiment shows (i) a crossing of the magnetization curves, reported at 2 and 5 K occurring at ~2 T, and (ii) a linear increase from 0 to 3 T, followed by a more pronounced increase with positive curvature at higher fields. These features are only observed when D is negative (Figure 16b). When D is positive or zero, the model predicts a nearly linear field dependence of the magnetization at these temperatures. Similar antiferromagnetic behavior has been observed in the two related compounds $Fe_2(NSC)_4(2,2'\text{-bpym})_3$[13a] and $Co_2(NSC)_4(2,2'\text{-bpym})_3$,[13b] although in these cases only the magnetic susceptibilities were analyzed, and the spin anisotropy was neglected, rendering a comparison of the deduced J values irrelevant. In these compounds, the temperatures of the maxima are quite similar to those obtained in the present case (12 and 16.4 K, respectively).

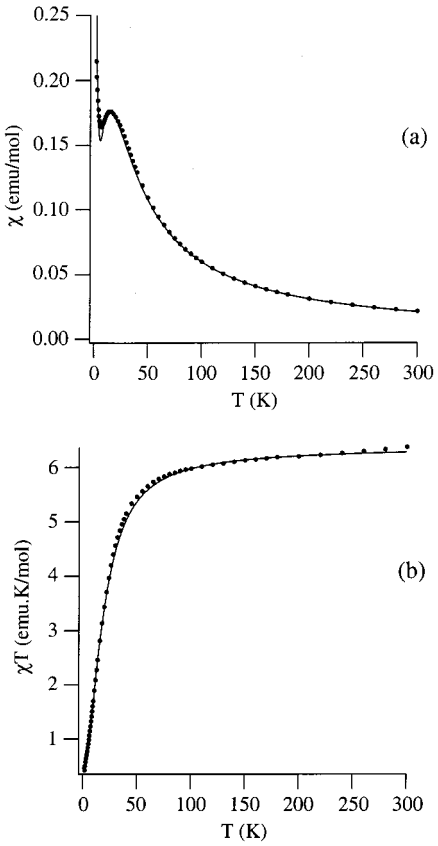

Figure 17. Thermal dependence of the susceptibility (a) and of the product χT (b) for $[Et_4N]Cl\cdot[Fe_2Cl_4(MeOH)_4(\mu\text{-}2,2'\text{-bpym})]$.

The compound $[Et_4N]Cl\cdot[Fe_2Cl_4(MeOH)_4(\mu\text{-}2,2'\text{-bpym})]$ (**9**) exhibits magnetic behavior that is similar to that of $Fe_2Cl_4(2,2'\text{-bpym})_3$, with a maximum in χ at ca. 20 K (Figure 17). The only noticeable difference concerns the observation of a larger Curie tail contribution at low temperatures, which merely indicates the presence of a larger quantity of $S = 2$ paramagnetic impurities in the sample. The magnetic data were satisfactorily fitted to the following set of parameters: $J = -1.0$ cm^{-1}, $D =$

(23) See, for example: de Jongh, J. L. In *Magneto-structural correlations in exchange-coupled systems*; Willett, R. D., Gatteschi, D., Kahn, O., Eds.; NATO ASI Series C 140; Reidel: Dordrecht, 1985; pp 1−35.

$-16.3\ cm^{-1}$, and $g = 2.07$, with a 7.5% impurity of monomeric Fe(II). As one can clearly see, the magnetic parameters associated with this Fe(II) compound are within the range of values obtained for compound **8**, in fairly good agreement with the structural resemblance of these two dimers.

Conclusions

The results of this study demonstrate that edge-sharing bitetrahedral anions of the type $[M_2Cl_6]^{2-}$ are readily synthesized for Mn(II), Fe(II), and Co(II). These dinuclear compounds represent soluble, molecular versions of the polymeric divalent metal chlorides, MCl_2, which exhibit the CdI_2-type structure. Although these compounds are chemically quite simple, their magnetic properties are of interest in light of the exchange coupling between the metal centers and the magnetic anisotropy. Regardless of the nature of the cations, the Fe series exhibits magnetic behavior that is dominated by the single-ion anisotropy of the tetrahedral Fe(II) centers with negligible coupling between the metal centers. The magnetic behavior of $[ppn]_2[Co_2Cl_6]$ is also anisotropic, and the antiferromagnetic coupling is much stronger as a consequence of the more acute Co−Cl−Co angles compared to the Fe−Cl−Fe angles. The behavior of $[ppn]_2[Mn_2Cl_6]$ is different from that of the other metal compounds due to the fact that the ground state is not affected by large zero-field splitting terms. In this case, more subtle effects of *intermolecular* as well as *intramolecular* interactions can be observed, because there are no complications arising from ZFS effects.

Reactions between 2,2′-bipyrimidine and two different salts of $[Fe_2Cl_6]^{2-}$ yield neutral products as a result of loss of two Cl^- ions from the coordination sphere. The new compounds, $Fe_2Cl_4(2,2'\text{-bpym})_3$ and $[Et_4N]Cl\cdot[Fe_2Cl_4(MeOH)_4(\mu\text{-}2,2'\text{-bpym})]$, contain Fe(II) centers bridged by a bis-chelating 2,2′-bpym ligand which mediates antiferromagnetic exchange. Fittings of the magnetic data required large and negative *D* parameters in order to reproduce the behavior. We are investigating these complexes as building blocks for extended arrays due to the presence of dangling 2,2′-bipyrimidine ligands in $Fe_2Cl_4(2,2'\text{-bpym})_3$ and to the presence of solvent molecules in axial positions in $Fe_2Cl_4(MeOH)_4(\mu\text{-}2,2'\text{-bpym})$.

Acknowledgment. K.R.D. gratefully acknowledges funding from the National Science Foundation (CHE-9622589) and the Center For Fundamental Materials Research at Michigan State University for support of a summer fellowship to J.M.C.-J. The work in Valencia has been supported by the Spanish Ministerio de Educación y Cultura (Grant PB96-0862). Funds for the diffractometers and the SQUID magnetometers used in this study were obtained from the National Science Foundation (for K.R.D.) and from the Ministerio de Educación y Cultura and the Generalitat Valenciana (for E.C.).

Supporting Information Available: Tables listing detailed crystallographic data, atomic positional parameters, and bond lengths and bond angles for **1**−**4** and **6**−**9**. This material is available free of charge via the Internet at http://pubs.acs.org.

IC990525W